IEEE Photonics Journal
An IEEE Photonics Society Publication

Open Access

Thermo Optic Coefficients and Electronic Polarizabilities of Tungsten Bronzes Using Ellipsometry

Volume 11, Number 6, December 2019

Zahid Hussain

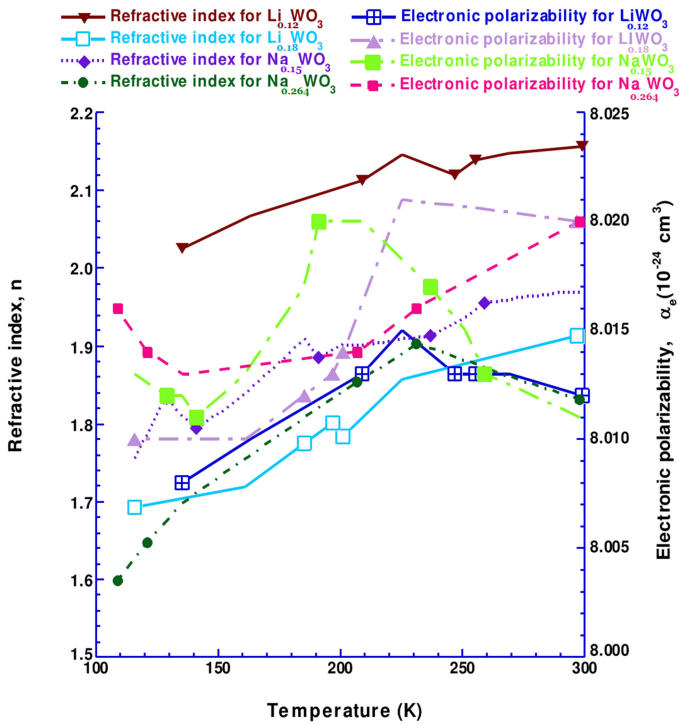

DOI: 10.1109/JPHOT.2019.2941755

IEEE photonics SOCIETY

IEEE

Thermo Optic Coefficients and Electronic Polarizabilities of Tungsten Bronzes Using Ellipsometry

Zahid Hussain

Imperial College of Science, Technology and Medicine, Department of Electrical and Electronic Engineering, London SW7 2BT U.K.

DOI:10.1109/JPHOT.2019.2941755

Manuscript received July 2, 2019; revised September 8, 2019; accepted September 10, 2019. Date of publication September 17, 2019; date of current version October 30, 2019. This work was supported by the EEE Department at Imperial College London by private fundings.

Abstract: The values of dn/dT for thermally evaporated WO_3 thin films were found to be negative either in the heating cycle (295–373 K) or in the cooling cycle (100–300 K) and were found to be of order of 10^{-5} K^{-1}. On the other hand thermo optic coefficients (TOCs: dn/dT and dk/dT values) of tungsten bronzes (H^+, Li^+, Na^+) with different concentrations were found to be positive and negative, respectively in both the heating and cooling cycles and they were found to be in the order of 10^{-4} K^{-1}. Heating cycles show hysteresis loops of n and k for tungsten bronzes, which are good for electrochromic devices. On heating the bronzes at temperature higher than 400 K, there might be a reduction in the porosity but an irreversible disordering of hydrogen, lithium or sodium atoms could occur because of anomalous dispersions produced in the optical data. For cooling cycles, the calculated TOCs were again of the order of 10^{-4} but there was an increase in dn/dT and a decrease in dk/dT values due to more amorphousness built up in the bronzes during the cooling cycles. This change in the values of TOCs for tungsten bronzes created small decrease in electronic polarizabilities (α_e) which were calculated in the range from 8.003 to 8.02 $\times$ 10^{-24} cm^3 in the cooling cycles.

Index Terms: Opto-electronics, electro-optical devices, electro-optical materials, optical properties, optical constants, optical devices, thin films.

1. Introduction

Electrochromism occurs in many organic materials and in transition metal oxides based on W, V, Mo etc. These electrochromic materials can be prepared by different deposition methods and used in different electrochemical devices such as electrochromic windows [1]–[3], energy storage devices [4], [5], gas sensors [6], [7] and chemical sensors [8], [9]. Since tungsten trioxide (WO_3) is a wide band gap semiconductor material that is used as an important electrochromic layer in electrochromic devices for reversible colour change [5], [10], researchers have widely studied WO_3 thin films and device applications [5], [11], [12].

There is keen interest in the use of amorphous or mirocrystalline WO_3 thin films as cathodic electrodes in transmittance-modulating electrochromic devices [13], [14]. WO_3, in thin film form, has novel properties such as great optical modulation, good durability, and low power consumption [6], [15], [16]. Due to these properties, WO_3 may be successfully used in photochromic [6], [17], gasochromic [7], [18], photo-catalyst [19], [20], photoluminescence properties [21], optical

memories, optical modulation, flat panel displays [22], [23],writing-reading-erasing optical devices [15], [24], humidity, temperature sensors [6], [7], and in microelectronic devices [25]–[27]. Tungsten trioxide is known to be quite reactive with basic compounds in forming various salts for various technical benefits [28], [29]. The discovery of high temperature super-conductivity has further intensified interest in research on perovskite oxides, especially tungsten trioxide and their bronzes [30], [31].Tungsten trioxide in thin film form has also been known to have other practical applications such as anti-dazzling rear-view mirrors for auto-mobiles [32]–[34], and non-emissive information displays [1], [35] due to its variable diffuse reflectance.

We have recently published papers on the optical constants and electrochromic characteristics of M_xWO_3 ($M = H^+$, Li^+, Na^+) and Z_xMoO_3 ($Z = H^+$, Li^+) bronzes using ellipsometry [36], [37], and our next interest is to publish some temperature dependent ellipsometric data on tungsten & molybdenum bronzes and also to explore some annealing effects on the optical properties of these bronzes in the temperature range $100 < T < 400$ K for electrochromic devices and for other technical applications.

In this paper, ellipsometry has been used as an optical technique to prepare temperature dependent optical data for tungsten bronze thin films in the visible range of solar spectrum. All the thin films were deposited on unheated 7059 glass substrates, which contain low amounts of Na, and have good coloring-erasing properties. Later on, the reported thin films were heated and cooled using vacuum cryostat over the temperature range 100–400 K to prepare ellipsometric data which will be highly useful for electrochromic devices and for other technical applications. There is a plethora of structural analysis in the literature that WO_3 thin films still remain microcrystalline when heated below 673 K whereas films heated above 673 K turn into crystalline phase [38]–[40]. It has also been concluded that amorphous or microcrystalline phase shows superior intercalation capability to crystalline phase [39], [40]. We have also observed the better electrochromic performance for the "as deposited room temperature prepared films" and also for the heat treated films over the temperature range 295–400 K.

The temperature dependent (n, k) data of the reported M_xWO_3 ($M = H^+$, Li^+, Na^+) bronzes has been analysed in terms of thermo optic coefficients, mass density, porosity, and electronic polarizability (α_e) for better technical applications. The reported data has also been interpreted using polaronic and bipolaronic excitations and transitions regarding structural transformations during heating and cooling treatments.

2. Ellipsometry

For ellipsometric measurements, the manual ellipsometer along with a cryostat was built up with a monochromatic light source (He-Ne laser with wavelength of 632.8 nm) and with single incidence angle (set at 60°). Vacuum cryostat was built up with the ability to heat and cool the samples over a broad range of temperature, i.e., $100 < T < 400$ K. The sample cell temperature was monitored through alumel-cromel thermocouple, and regulated by a controller. The setup and procedure have been described in detail elsewhere [41], [42], [45].

In this work, the 3 phase model film/substrate/ ambient, all isotropic, is used. Which, in general, in terms of two ellipsometric measured angles (ψ and Δ), can be mathematically represented by [43], [44]

$$r(n_0, n_f, k_f, n_s, d, \phi, \lambda) = \frac{|r_p|}{|r_s|} e^{j(\delta_p - \delta_s)} \tag{1}$$

$$\text{where} \quad \tan\psi = \frac{|r_p|}{|r_s|} = |\rho|\,, \tag{2}$$

$$\text{and} \quad \Delta = \delta_p - \delta_s. \tag{3}$$

Where $|\rho|$ is the ratio of magnitudes of the Fresnel complex reflection coefficients r_p and r_s between the p (parallel) and s (normal) polarization states. In Eqs. (2) and (3), *tan* ψ*(or* $|\rho|$*)* is the

amplitude ratio and Δ the relative phase shift between p and s components. Experimentally, we measure Ψ and Δ which are the conventional ellipsometric angles associated with the angles of the optical components P (Polarizer), C (Quarter-wave plate), and A (Analyzer) of the manual nulling ellipsometer.

In Eq. (1) n_o, n_f, n_s are the real refractive indices of the air, film, substrate, respectively, and $\boldsymbol{k_f}$ is the extinction coefficient of the film;d, ϕ, and λ, are the thickness of the film, angle of incidence, wavelength, respectively.

It should be noted that the Fresnel equation (1) is a quintic polynomial equation for which exact inverse equation even for a single-wavelength and single-angle of incidence ellipsometry (set up for an isotropic 3 phase model film/substrate/ambient) cann't be written. Some quintics may be solved in terms of radicals or using trigonometry, but the solution is generally too complex to be used in practice.

Instead, numerical models can be calculated using root-finding algorithms (from literature) for polynomial equations in case of an absorbing film on an absorbing substrate or for the case when the substrate is a dielectric with an absorbing film.

Most optical models (numerical algorithms) use iteration (or regression) scheme to find the best match between model and experiment. Generally, in order to calculate ρ, one has to find the unknowns which are the thickness d, the refractive index n_f and the extinction coefficient of the film (k_f). The other parameters (n_0, n_s) are all known during the experiment. Using an algorithm with its iterative procedure (least-squares minimization) unknown optical constants and /or thickness parameters are varied, and Ψ and Δ values are calculated using equations (1), (2), and (3). The values of the parameters are adjusted to minimize the difference between the measured and calculated spectra by linear regression. The minimum between the data curves (model and experiment) is quantified with the help of an estimator like the Mean Squared Error (MSE). And the lowest MSE is equivalent to the best answer.

In our case, we have not developed any analytical inversion model or any iteration scheme based algorithm or any mathematical model for the numerical analysis of our experimental ellipsometric data, because that theoretical work was not (and is not) a part of our research project. Rather, we have developed Fortran 77 {an improved version of McCrackin package [44] to compute the values of n_f and k_f for different values of thickness (d), determined by an independent technique (Talysurf technique) [46].

3. Preparation of Specimens and Determination of X-Values

3.1 Preparation of Tungsten Bronze Thin Films

Li_xWO_3 (or Na_xWO_3) films were prepared by co-deposition of lithium and WO_3, evaporated from separate sources due to large difference in their vapour pressures. A silica boat was used for WO_3, and lithium (or sodium) metal was evaporated from a separate resistivity-heated "molybdenum boat." Substrates (on silica slides for spectroscopic work, and on I.T.O glass substrates for electrochemical extraction) were positioned on the deposition platform so as to minimize compositional variations. The final base pressure was 5×10^{-6} Torr, and was decreased to $\sim 10^{-7}$ torr by liquid nitrogen cold trap filled. WO_3 and Li (or Na) were outgassed for 30 minutes at 1123 K and 353 K (or 373 K for Na), respectively prior to evaporation. During deposition the chamber pressure was low, $< 10^{-7}$ Torr because of the gettering action of the lithium (or sodium) for all gases other than the noble gases. It is perhaps useful to note that the lithium metal pellets are normally covered in an almost black lithium nitride skin (unlike sodium metal which is covered in a colourless oxide skin). When the temperature of the WO_3 powder was raised up to the point where steady evaporation rate 15–16 Å sec^{-1} was reached, and the evaporation rate of Li (or Na) was steady the shutter covering the substrates (7059 glass and I.T.O glass slide) was then opened, and deposition of the WO_3 film started. Li (or Na) was also allowed to evaporate on the same substrates. Bronzes of different concentrations (or x-values) were obtained by controlling the rate of evaporation of Li (or Na) metal, and varying the time for their depositions. More details are given elsewhere [46], [47].

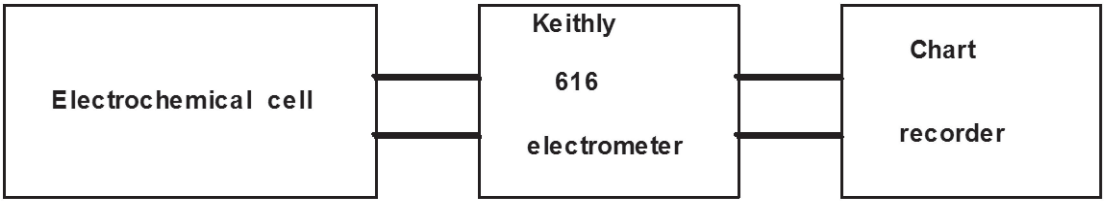

Fig. 1. Schematic diagram for the experimental arrangement for guest atom concentration determination.

Hydrogen tungsten bronzes were prepared by passing hydrogen plasma into the WO_3 film at the pressure of 6×10^{-1} torr. The atomic hydrogen was formed by means of a microwave discharge in the vecuum/gas-handling system. The system was evacuated to a pressure of 10^{-3} torr, and then filled with spectroscopic grade ($\sim$1-ppm impurity) hydrogen gas to a pressure of 0.1 torr. A "Microtron 200" microwave generator with tunable cavity was used and the discharge was initiated using a tesla coil. The films {on silica slides for spectroscopic work, and on I.T.O glass substrates for electrochemical extraction} were heated to about 373 K and were away about 25 cm from the atomic hydrogen bronze source. The resulting concentration of the hydrogen bronze was roughly proportional to exposure time, and it took 3-4 min to form hydrogen tungsten bronze with $x = 0.14$ in a 0.3-μm thick WO_3 film. A full description of the apparatus and the preparation technique are given elsewhere [47], [48].

The thickness of each film was measured four times using a Talysurf Mechanical Profilometer to determine an average value with a standard deviation of $\pm$30 Å. Grain size as observed by transmission electron microscopy (TEM) and X-ray diffraction techniques, has a range 20–80 Å (giving a mean grain size $\sim$50 Å). The same conclusions were reached by other researchers [49]–[51]. The density of evaporated WO_3 was determined to be 6.0 ± 0.3 gm/c.c [41], [47]. Tungsten oxide films evaporated from WO_3 powder (at room temperature) have been reported to be defect compounds of the type WO_{3-y}, and the stoichiometry of the evaporated WO_3 thin films was reported to be $\sim$2.72 (O/W ratio) by many workers [from different techniques, e.g., Proton backscattering, Auger electron spectroscopy (AES) and Electron spectroscopy for chemical analysis (ESCA)] [52]–[54].

3.2 Determination of X-Values Using Electrochemical Extraction Technique

There are two different sets of techniques which one can use to measure the hydrogen or lithium or sodium content of M_xWO_3 ($M = H^+$, Li^+, Na^+) films, and these are chemical and electrochemical. Chemical techniques have not been used because of the following restrictive measure. Any chemical method involves the destruction of the film which is under examination and therefore one has to take all other physical measurements before the x-value is determined. Since H or Li out-diffuses continuously from the films, the determination of x-values after the measurement of other physical properties, severely limits its usefulness, therefore, the concentration, x, was determined using an electrochemical method [47], [48], [51].

The electrochemical cell built-up with a propylene carbonate solution of $1M|1\ LiClO_4$ as the electrolyte has the following configuration:

$$C_1, \text{I.T.O}, M_xWO_3 \text{ bronze} \,\big|1M \text{ Li } ClO_4\big|\, \text{Pt}, \ C_2, \tag{4}$$

here C_1 and C_2 are electrical connections and Pt is a platinum wire electrode. The extraction of guest content, M atom, was performed under constant current (10^{-5}A cm^{-2}) conditions. A Keithley 616 electrometer was used as the constant current source while the potential difference between the two electrodes ($LiClO_4$ solution and platinum counter electrode) was continuously recorded on a JJ instrument 550 chart recorder. Schematic diagram of the apparatus used for the determination of x-values is shown in Fig. 1. Two films were prepared from the same evaporation run. One was

deposited on a silica substrate and was used for optical and electrical measurements, and the other on an Indium Tin Oxide (I.T.O) coated glass slide and was used for the guest concentration measurement.

During the insertion and extraction of hydrogen (or lithium) under constant current conditions, the voltage of the working electrode with respect to the platinum reference electrode was monitored to ascertain that the end of the extraction process was sharply profiled.

What we want to know is the x value within the grains, as the guest atom is taken to reside in the grains and not along the grain boundaries of microcrystalline WO_3 thin film. This notion is consistent with the expected ratio of (interior) surface-to-grain binding energy for a guest atom. It is supported by the grain-size-independent (for small regime) optical properties in the "blue-band" range. It is in accord with the diffusion behavior, which is rapid in the grain-boundary manifold and slow in the grains. The value of x within the grains (mean grain size $\sim$5 nm) has to be calculated on the basis of 1.0×10^{22} H^+ (or Li^+) ions cm^{-3} being equivalent to $x = 1$ when the coulombmetric titration technique is used. The exact amount, x, that was extracted, was determined from the numerical model described below.

Determination of concentration x is based on the electrochemically reversible formation of a tungsten bronze thin film according to double injection of positive ions and electrons, namely,

$$(\text{colorless})\, WO_3 + xM^+ + xe^- \rightarrow M_xWO_3\, (\text{blue color})\,, \tag{5}$$

where $0 < x < 1$ and M (H, Li, Na, etc) is the guest atom inserted into WO_3.

The concentration x is defined as the ratio of number of moles of guest atom to the number of moles of WO_3. If we use the experimentally determined film density, ρ_f what we can determine, from electrochemical extraction is an average x-value, $\langle x \rangle$, defined as [46], [47], [49]

$$\langle x \rangle = \frac{N_T M}{A \rho_f V_f}, \tag{6}$$

where N_T is the total number of guest atoms present in a volume V_f of a WO_3 thin film of density ρ_f, M is the molecular weight, and A is Avogadro's constant.

If we assume that the density of the WO_3 thin film is the same as the single-crystal density and suppose that the injected amount of hydrogen (or lithium) in a film, at equilibrium, is in the grain as a result of its high binding energy, the x value in the grain will then be given by

$$x = \frac{N_T M}{A \rho_s V_G}, \tag{7}$$

where V_G is the volume of the film that is grain, as distinct from the volume ascribed to the grain-boundary regions (V_{GB}), and ρ_s is the WO_3 single-crystal density (7.3 g/cc).

The total charge removed from known volume V_f of the film is given by

$$Q_T = I t_f, \tag{8}$$

where I is the constant current flowing through the cell and t_f is the time for extraction until the end of the bleaching process. In as much as every guest atom removed is singly ionised, the total number of guest ions extracted is

$$N_T = \frac{Q_T}{e}, \tag{9}$$

where e is the electronic charge.

For the same value of N_T, Eqs. (6) and (7) can be combined as

$$x = \langle x \rangle \frac{\rho_f V_f}{\rho_s V_G}. \tag{10}$$

Because

$$V_f = V_G + V_{GB}, \tag{11}$$

i.e., the volume of film equals the volume of the grain and the volume of grain boundary, so Eq. (10) can be rewritten as

$$x = \langle x \rangle \frac{\rho_f}{\rho_s}\left(1 + \frac{V_{GB}}{V_G}\right). \tag{12}$$

It is clear that x, apart from the density of the film, also depends on the ratio V_{GB}/V_G. Let the mean grain size be L and the thickness of the grain boundary be l (where $l << L$); then V_G can be expressed as

$$V_G \propto L^3,$$

and

$$V_{GB} \propto L^2 l.$$

Combining both leads to

$$\frac{V_{GB}}{V_G} = \frac{constant.l}{L}$$

or

$$\frac{V_{GB}}{V_G} = \frac{\sigma}{L}. \tag{13}$$

So Eq. (12) can be rewritten as

$$x = \langle x \rangle \frac{\rho_f}{\rho_s}\left(1 + \frac{\sigma}{L}\right), \tag{14}$$

where σ is the product of the grain boundary thickness l and some geometrical factor, that depends on the shape of the grains. The value of σ was found to be $\sim 44 \pm 3$ Å from the thermodynamic data [47], [51]. L, the mean grain size of WO_3 was found by electron diffraction studies to be 50 ± 10 Å [47], [51].

From Eqs. (6), (8), (9), and (14), the expression for x can be reshaped as

$$x = \frac{l\, t_f M}{e V_f A\, \rho_s}\left(1 + \frac{\sigma}{L}\right). \tag{15}$$

Using the following values:

$$\begin{aligned} l &= 10^{-5}\ \text{A/cm}^2, \\ M &= 231.85\ \text{g/mol}, \\ \text{e} &= 1.6 \times 10^{-19}\ \text{C}, \\ \text{A} &= 6.022 \times 10^{23}\ \text{mol}^{-1} \\ \rho_s &= 7.3\ \text{g/cm}^3, \\ \rho_f &= 6.0 \pm 0.3\ \text{g/cm}^3, \\ \sigma &= 44 \pm 3\ \text{Å}, \\ L &= 50 \pm 10\ \text{Å}, \end{aligned}$$

and substituting all these values back into Eq. (15), we can finally obtain the numerical expression as

$$\text{x} = 6.19 \times 10^{-15}\left(\text{cm}^3/\text{s}\right)\left(\frac{\text{t}_f}{\text{V}_f}\right)\left(\text{s/cm}^3\right),$$

or

$$x = 6.20 \times 10^{-15} \frac{t_f}{V_f}. \tag{16}$$

Where t_f is the time for extraction until the end of bleaching process, and V_f indicates the extracted volume of the thin film. Equation (16) was our numerical model, which was successfully applied even to high values of hydrogen (ions) or lithium or sodium (metal) ions inserted into WO_3 thin films.

The values of t_f and V_f were both determined experimentally for each film under study. The volume of the extracted part of a film required a determination of thickness and area, which were measured, respectively, by a Taylor-Hobson Talysurf profilometer and an optical microscope to a precision of greater than 4%. Taking into account the uncertainties in the measurements of extracted volume and also in the values of σ and L yields a relative accuracy of $\pm 6\%$ in the calculation of x-values. The overall absolute accuracy in the x values with Eq. (16) is correct to within $\pm 10\%$.

4. Experimental Results and Error Analysis

Before the use of computer program, four zone averaging of extinction settings for Polarizer and Analyzer is usually needed to reduce the instrumental imperfections and other systematic errors [41], [44].In order to do that, we used different combinations of P, C and A at null, which are linked to ellipsometric angles Δ and Ψ by the relations [41], [43], [44]

$$\boldsymbol{\Delta}_i = \pm \mathbf{2}\boldsymbol{P}_i \pm \mathbf{90}^o, \tag{17}$$

and

$$\boldsymbol{A}_i = \pm \boldsymbol{\Psi}_i. \tag{18}$$

Where i = 1, 2, 3, 4 are the numbers for four zones.

Once the ellipsometric measurements of Δ and Ψ were determined, the next stage was to compute the values of n_f and k_f using equations (1)–(3) for the reported tungsten bronzes with different values of thickness (d). Temperature dependent data for WO_3 and for M_xWO_3 bronzes were computed in the range $295 \leq T \leq 373$ K, and are printed in Tables 1–4. Their respective plots of (n, k) vs temperature (along with error bars) are shown in Figs. 2–5.

Ellipsometric data on WO_3, H_xWO_3, Li_xWO_3 and Na_xWO_3 {over the temperature range $100 < T \leq 298$ K} are printed in Tables 5–11. Plots of (n, k) vs temperature (along with error bars) for WO_3 and its bronzes are displayed in Figs. 6–12 with solid line-curve fittings to expose their common trend. Periods of time taken for different data points are also shown in the reported figures.

The standard deviation of the readings (at room temperature) gave $\pm 0.02^o$ for $\delta\Psi$ and $\pm 0.03^o$ for $\delta\Delta$, resulting an error of about $\pm 0.2\%$ in n and an error of about $\pm 0.1\%$ in k. The values of $\delta\Delta$ and $\delta\Psi$ relating to systematic, random and the birefringence effects in cell window, were collectively found to be within $\pm 0.04^o$ and 0.02^o, respectively.

The maximum spread in the angle of incidence was taken as $\pm 0.07^o$ during cooling and heating cycles.

In the temperature range $295 \leq T \leq 373$ K, the maximum errors in n and k were found to be of about ± 0.0012 and ± 0.0012, respectively. Similarly, in the range $100 < T < 350$ K, a relative change of 0.02^o in Ψ caused an error in n of about $\delta n = \pm 0.0031$. A relative change of 0.23^o in Δ produced a change in k of about $\delta k = \pm 0.0012$.

Full details of error analysis are given in Tables 12 and 13.

5. Discussion

5.1 Crystalline Structural Models and Conduction Processes in WO_3 and in Their Bronzes

At room temperature, WO_3 exists as a three dimensional distorted ReO_3 type crystal, and normally has unit cell parameters, a = 7.31 Å, b = 7.54 Å, and c = 7.952 Å, as shown in Fig. 13. It has four short and two long bond lengths in each octahedral [55]. This monoclinic structure contains eight

TABLE 1

Vacuum-Ellipsometric Data on WO_3 Thin Film in the Temperature Range 297 ≤ T ≤ 373 K

Thickness=0.30μm ϕ=60.34°				
Temperature (K)	**Δ (°)**	**Ψ (°)**	**n**	**k**
Heating cycle				
297.0	6.92	5.46	2.0018	0.00015
333.0	10.25	5.44	1.9997	0.00020
373.0	13.12	5.67	1.9978	0.00049
Cooling cycle				
333.0	9.14	5.58	2.0039	0.00029
297.0	6.86	5.40	2.0019	0.00030

TABLE 2

Vacuum-Ellipsometric Data on H_xWO_3 Bronze Thin Film in the Temperature Range 297 ≤ T≤ 73 K

Thickness=0.435μm x=0.12 ϕ=60.33°				
Temperature (K)	**Δ (°)**	**Ψ (°)**	**n**	**k**
Heating cycle				
298.0	164.42	4.30	1.9477	0.11367
333.0	165.33	4.31	1.9487	0.11250
373.0	165.75	4.26	1.9478	0.11172
Cooling cycle (back to room temperature)				
297.0	159.89	4.33	1.9428	0.11924

TABLE 3

Vacuum-Ellipsometric Data on Li_xWO_3 Bronze Thin Film in the Temperature Range 295 ≤ T ≤ 373 K

Thickness=0.29μm x=0.313 ϕ=60.34°				
Temperature (K)	**Δ (°)**	**Ψ (°)**	**n**	**k**
Heating cycle				
295.0	107.28	8.28	1.7853	0.24815
333.0	108.63	8.14	1.7937	0.24356
373.0	109.14	8.27	1.7969	0.24639
Cooling cycle				
333.0	108.83	8.35	1.7950	0.24864
295.0	106.99	8.42	1.7831	0.25186

TABLE 4
Vacuum-Ellipsometric Data on Na_xWO_3 Bronze Thin Film in the Temperature Range 298 ≤ T ≤ 373 K

Thickness=0.22μm x=0.105 $\phi=60.34^{o}$				
Temperature (K)	**Δ (^{o})**	**Ψ (^{o})**	**n**	**k**
Heating cycle				
298.0	174.50	0.32	2.0938	0.06289
333.0	173.15	0.24	2.0926	0.06201
373.0	172.37	0.11	2.0910	0.06055
Cooling cycle (back to room temperature)				
298.0	171.85	0.10	2.0909	0.06045

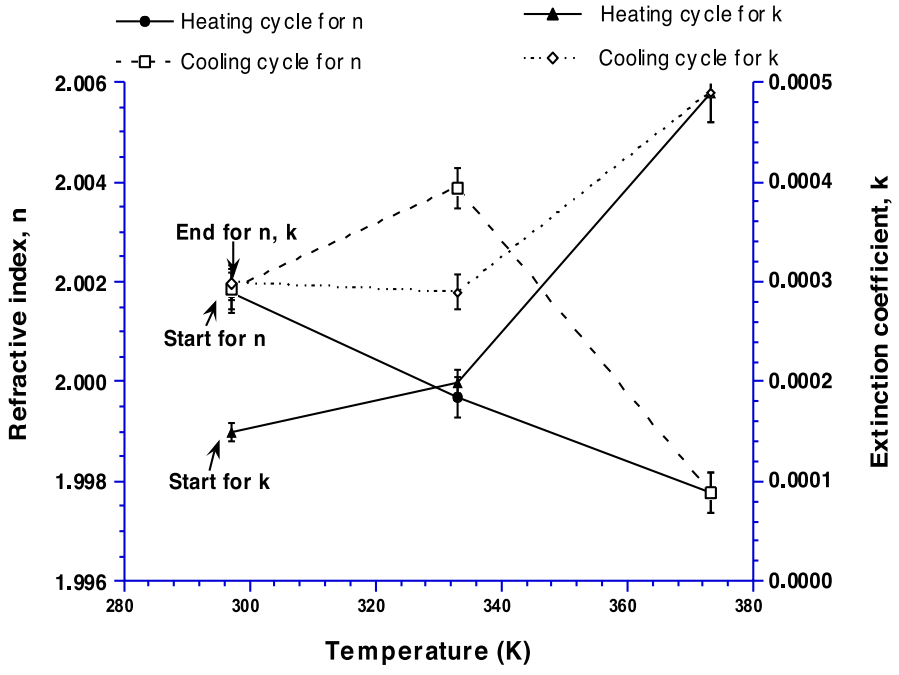

Fig. 2. Plot of (n, k) versus temperature, T, of WO_3 thin film under vacuum in the range 297–373 K.

WO_3 units per cell [56], and belongs to the space group $\mathbf{C_{2h}^5}$. However, below room temperature, due to ferroelectric (or anti-ferroelectric) distortion of the WO_6 octahedra, another crystallographic phase possibly triclinic (ReO_3 type) structure [57] {with unit cell parameters, a = 7.31 Å, b = 7.68 Å} exists, as shown in Fig. 14. Crystalline tungsten bronzes of M_xWO_3 ($M = H^+$, Li^+) also occur in a hexagonal, monoclinic, tetragonal, or perovskite related cube structures with a network of corner sharing tungsten-oxygen octahedral in the concentration range $0 < x < 1$ [58], [59]. For the values of x in the upper portion of the range $0 < x < 1$ (say for $x > 0.4$), many of the tungsten bronzes,M_xWO_3 ($M = Li^+$, Na^+) take on a cubic perovskite-like structure [60], [61] with all W-O bond lengths equal like a ReO_3 unit as shown in Fig. 15(a). The cubic unit cell is also shown in Fig. 15

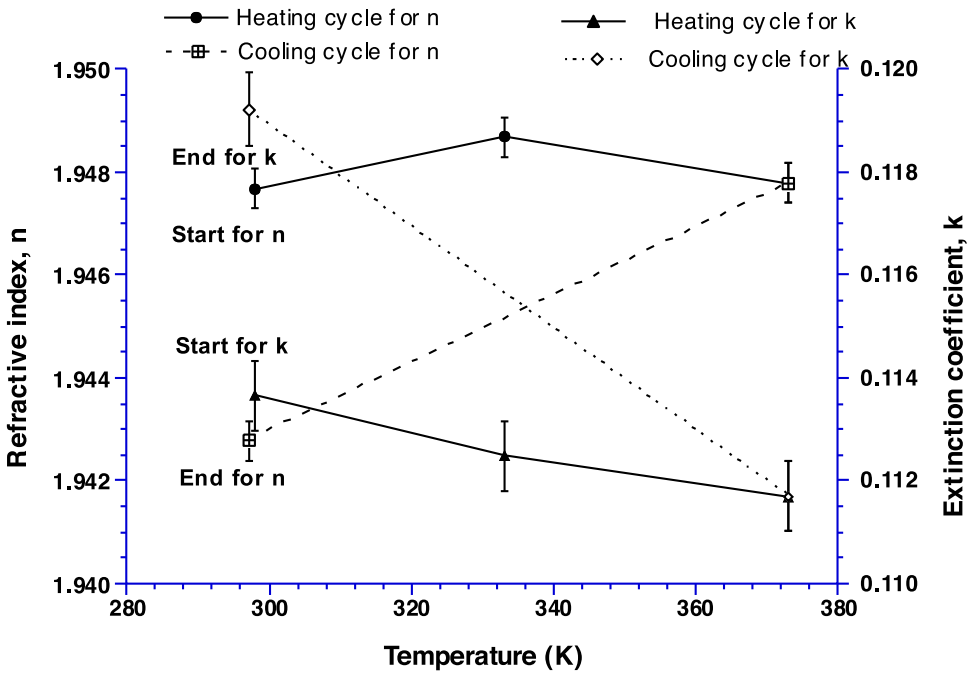

Fig. 3. Plot of (n, k) versus temperature, T, of $H_{0.12}WO_3$ bronze thin film under vacuum in the range 297–373 K.

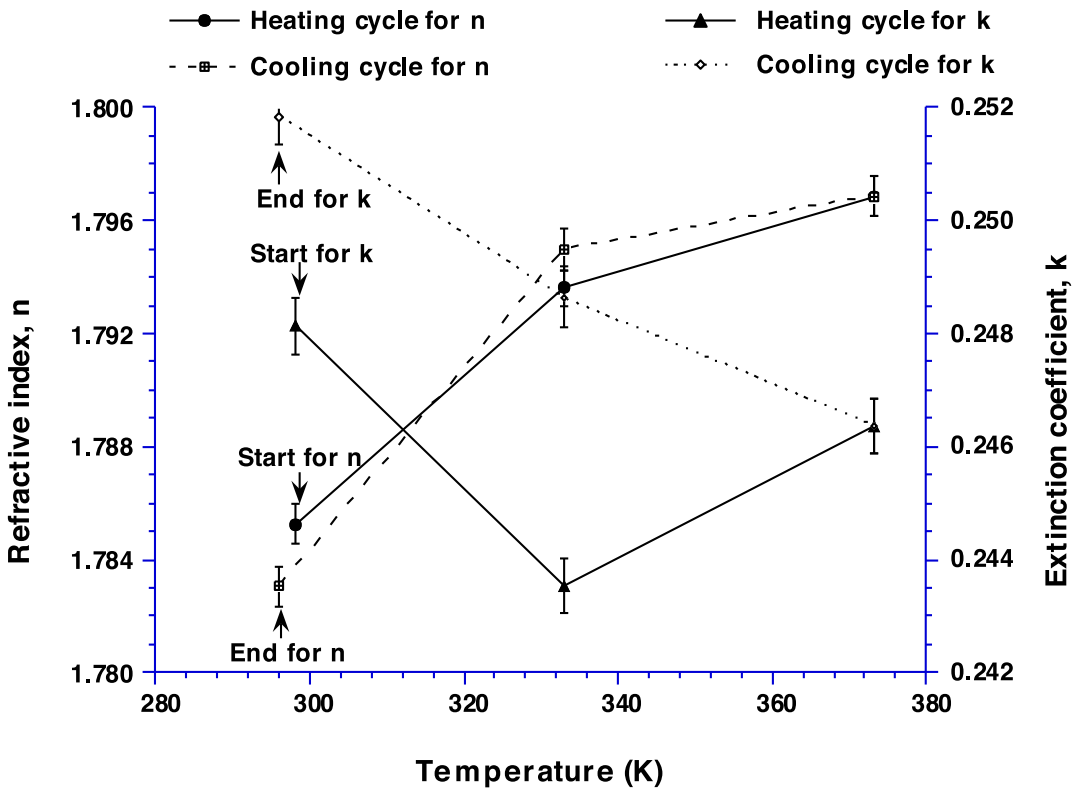

Fig. 4. Plot of (n, k) versus temperature, T, of $Li_{0.313}WO_3$ bronze thin film under vacuum in the range 297–373 K.

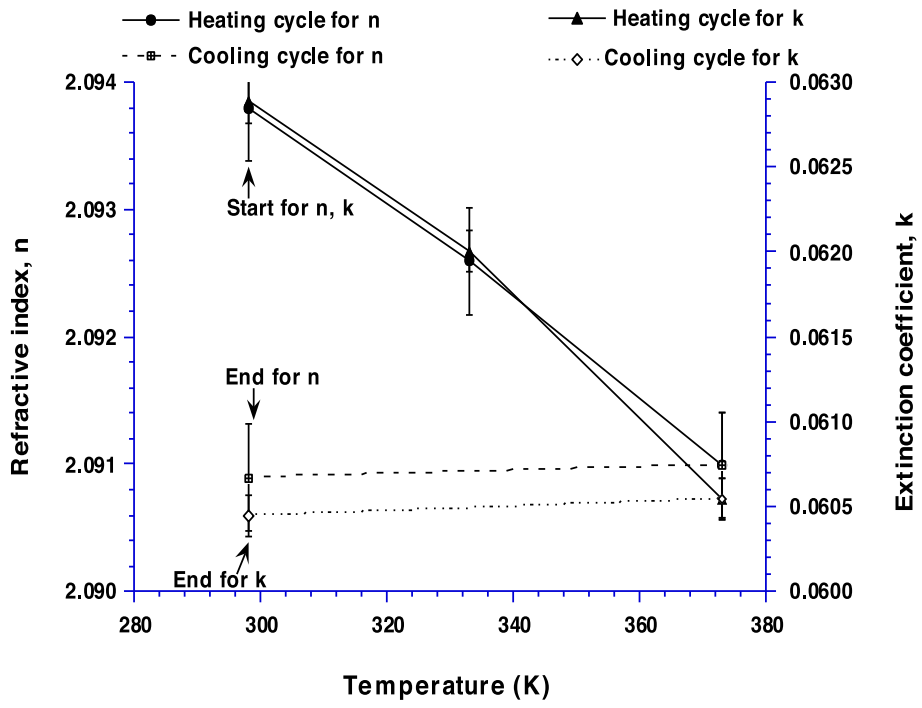

Fig. 5. Plot of (n, k) versus temperature, T, of $Na_{0.105}WO_3$ bronze thin film under vacuum in the range 298–373–K.

TABLE 5

Vacuum-Temperature Dependent Ellipsometric Data on WO_3 Thin Film Using Liquid Nitrogen as a Coolant, and Directing the Temperature with a 407 Controller

Thickness=0.26μm $\phi=60.34^{o}$				
Temperature (K)	**Δ (^{o})**	**Ψ (^{o})**	**n**	**k**
First cooling cycle				
297.0	40.80	6.65	2.0342	0.00801
197.0	28.86	6.11	2.0522	0.00381
191.0	28.34	6.53	2.0524	0.00782
163.0	27.88	5.75	2.0551	0.00039
Second cooling cycle				
213.0	29.23	6.00	2.0516	0.00273
175.0	28.64	5.87	2.0532	0.00146
157.0	28.44	6.41	2.0524	0.00674
137.0	26.69	5.63	2.0579	0.00059
125.0	25.43	5.76	2.0599	0.00088
111.0	23.46	5.98	2.0634	0.00012
Heating cycle (back to room temperature)				
229.0	33.92	6.03	2.0414	0.00234
267.0	33.32	5.94	2.0431	0.00246
297.0	34.17	6.18	2.0403	0.00381

TABLE 6

Vacuum-Low-Temperature Ellipsometric Measurements on H_xWO_3 Thin Film in the Temperature Range $100 < T \leq 373$ K*

Thickness=0.215μm x=0.15 ϕ=60.34°					
Temperature (K)	**Time (h)**	**Δ (°)**	**Ψ (°)**	**n**	**k**
Cooling cycle					
298.0		145.54	4.50	1.9221	0.13790
253.0		140.41	4.61	1.9128	0.14522
245.0		138.90	4.64	1.9098	0.14727
175.0		122.52	5.96	1.8772	0.18750
139.0		114.32	6.71	1.8456	0.21065
Heating cycle					
211.0		126.50	5.36	1.8852	0.17207
225.0		129.52	5.14	1.8921	0.16514
249.0		139.85	4.70	1.9134	0.14707
265.0	2.0	149.75	4.44	1.9291	0.13242
271.0		145.44	4.62	1.9247	0.13965
298.0	2.0	164.42	4.30	1.9451	0.11358
373.0		165.33	4.29	1.9487	0.11250
373.0	2.0	154.42	4.42	1.9369	0.12666
Cooling back to room temperature					
297.0		159.89	4.33	1.9428	0.11924

*The sample is heated up to 373 K and then cooled down to room temperature before readings are taken.

TABLE 7

Vacuum-Low-Temperature Ellipsometric Measurements on H_xWO_3 Thin Film in the Temperature Range $100 < T < 373$ K*

Thickness=0.27μm x=0.26 ϕ=60.32°					
Temperature (K)	**Time (h)**	**Δ (°)**	**Ψ (°)**	**n**	**k**
First cooling cycle					
323.0		105.51	8.01	1.8126	0.24649
135.0		96.02	11.29	1.6982	0.33194
121.0	2.0	93.61	12.70	1.6465	0.37012
First heating cycle					
297.0	2.0	133.85	5.08	1.9311	0.16231
323.0	2.0	133.92	4.97	1.9293	0.16045
Second cooling cycle					
249.0		127.24	5.51	1.9143	0.17647
237.0		126.02	5.35	1.9081	0.17442
231.0	1.0	125.49	5.15	1.9043	0.17100
109.0	2.0	92.53	14.19	1.5977	0.41367
Second heating cycle					
207.0		112.00	7.18	1.8535	0.22393
219.0		114.57	6.28	1.8666	0.20186
298.0	1.0	108.25	7.71	1.8307	0.23828

*Sample is heated up to 373 K and then cooled down to room temperature before readings are taken.

TABLE 8

Vacuum-Low-Temperature Measurements on Li_xWO_3 Thin Film in the Temperature Range $100 < T < 373$ K

Thickness=0.29 μm x=0.12 $\phi=60.34^o$					
Temperature (K)	**Time (h)**	**Δ (^{o})**	**Ψ (^{o})**	**n**	**k**
First heating cycle					
298.0		167.40	10.03	2.1565	0.12149
333.0		169.97	9.89	2.1509	0.11338
353.0		168.84	9.75	2.1452	0.11729
353.0	1.00	170.41	9.67	2.1420	0.11260
First cooling cycle					
209.0	0.50	149.38	9.98	2.1127	0.18867
163.0	0.25	142.36	9.78	2.0665	0.21270
135.0	0.50	136.92	9.60	2.0253	0.22822
Second heating cycle					
225.0		155.37	10.19	2.1456	0.16631
298.0	1.00	171.23	9.74	2.1445	0.10987
Second cooling cycle					
247.0	1.00	153.53	7.97	2.1193	0.17539
Second heating cycle (back to room temperature)					
255.0	1.0	156.50	8.24	2.1395	0.17090
269.0	1.0	162.85	7.90	2.1483	0.15244
298.0		164.70	8.07	2.1592	0.14912

TABLE 9

Vacuum-Low-Temperature Ellipsometric Measurements on Li_xWO_3 Thin Film in the Temperature Range $100 < T < 300$ K∗

Thickness=0.24μm x=0.18 $\phi=60.34^o$					
Temperature (K)	**Time (h)**	**Δ (^{o})**	**Ψ (^{o})**	**n**	**k**
First cooling cycle					
297.0		133.86	6.50	1.9138	0.17735
191.0	0.50	108.83	9.10	1.8009	0.26992
175.0	0.50	106.14	10.26	1.7750	0.30293
153.0	0.75	101.58	11.77	1.7191	0.34809
115.0	1.00	101.43	13.27	1.6931	0.39395
First heating cycle					
298.0	2.00	133.81	6.38	1.9106	0.17549
Second cooling cycle					
225.0	0.25	118.43	7.53	1.8568	0.22129
217.0	0.50	110.76	8.19	1.8146	0.24531
195.0	0.50	106.14	8.74	1.7836	0.26270
Second heating cycle (back to room temperature)					
298.0	2.00	131.92	6.28	1.9011	0.17696

∗The sample was heated up to 453 K and then cooled down to room temperature before readings were taken.

(b), with a tungsten atom at the centre, six oxygen atoms at face centres. For low x-values ($x < 0.4$), orthorhombic, tetragonal and hexagonal phases can exist, which are related to the perovskite phase and exhibit low symmetry structure [62], [63]. When these sites are completely empty, x in M_xWO_3 is zero and the structure resembles to that of WO_3. There is a reversible structural transformation from monoclinic to cubic with no broken chemical bonds, and this first order phase transition is

TABLE 10

Vacuum-Low-Temperature Ellipsometric Measurements on Na_xWO_3 Thin Film in the temperature range $100 < T \leq 373$ K*

Thickness=0.20 μm x=0.15 $\phi=60.34^o$					
Temperature (K)	**Time (h)**	**Δ (^{o})**	**Ψ (^{o})**	**n**	**k**
First heating cycle					
298.0		144.10	4.72	1.9694	0.14688
373.0	0.50	143.44	5.07	1.9749	0.15264
First cooling cycle					
259.0	0.50	135.36	5.36	1.9553	0.16621
209.0	1.00	119.47	6.35	1.9015	0.20010
116.0	1.00	99.37	10.08	1.7533	0.29912
Second heating cycle					
298.0	2.00	140.54	5.09	1.9669	0.15620
Second cooling cycle					
161.0	0.25	108.58	8.04	1.8404	0.24571
141.0	1.00	103.41	9.33	1.7938	0.27979
135.0	1.00	106.30	9.67	1.8108	0.28858
129.0	1.00	109.22	9.81	1.8321	0.29121
Third heating cycle (back to room temperature)					
185.0	1.00	120.76	6.64	1.9088	0.20547
191.0		115.98	6.30	1.8853	0.20117
201.0	0.75	119.73	6.53	1.9034	0.20391
237.0		122.41	6.17	1.9138	0.19405
251.0	1.00	128.88	5.86	1.9384	0.18194
297.0	2.00	142.01	4.92	1.9678	0.15205

*The sample is heated up to 373 K and then cooled down to room temperature before readings are taken.

TABLE 11

Vacuum-Low-Temperature Ellipsometric Measurements on Na_xWO_3 Thin Film in the Temperature Range $100 < T < 373$ K

Thickness=0.215μm x=0.264 $\phi=60.34^o$					
Temperature (K)	**Time (h)**	**Δ (^{o})**	**Ψ (^{o})**	**n**	**k**
First heating cycle					
298.0		108.25	7.71	1.8308	0.23828
333.0	8.0	114.57	6.28	1.8666	0.20186
First cooling cycle					
135.0	1.0	96.00	11.29	1.6982	0.33194
121.0	1.0	93.61	12.70	1.6465	0.37012
109.0	1.0	92.53	14.19	1.5977	0.41367
Second heating cycle (back to room temperature					
207.0		112.00	7.18	1.8535	0.22393
231.0	1.0	124.08	5.58	1.9031	0.18047
298.0	2.0	105.51	8.01	1.8126	0.24649

very suitable for the electrochromic characteristics of crystalline Li_xWO_3 and Na_xWO_3 bronzes [64], [65]. Elastic and inelastic neutron scattering studies on crystalline H_xWO_3 ($0 < x < 0.6$) bronze revealed a similar structure like a distorted ReO_3 lattice [66]–[68], but it is based on isolated–OH groups (for $x > 0.4$) [67], [69]. Stability of a particular structure will depend on the free energy of the M atoms in that structure; and moreover, it is also influenced by the temperature. On the higher

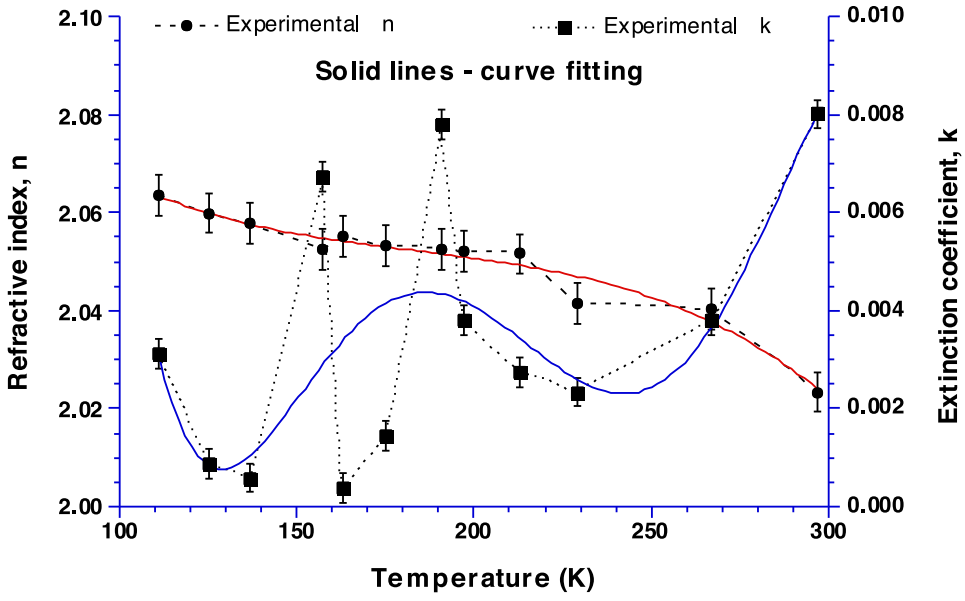

Fig. 6. Plot of (n, k) versus temperature, T, of WO_3 thin film under vacuum in the range 100–297–K.

range of the x-values ($x > 0.4$), a cubic (perovskite type) structure exists [70], one electron to the WO_3 matrix conduction band: mainly consisting of 5d orbitals of W atoms and pπ orbitals of oxygen atoms. Conduction takes place normally in a matrix delocalized band, and is of Bloch type. On the other hand, microcrystalline (or amorphous) tungsten bronzes are thought to be composed of WO_6 octahedra, and might be arranged in haphazardly packed clusters [71].They do not exhibit Bloch type characteristics due to their complex tungsten-oxygen networks. These microcrystalline bronze thin films have impurity (absorption) band or small polaron band in the matrix band gap, which is filled through electron exchanges (by hopping mechanism) among the neighbouring sites ($W^{6+} \longleftrightarrow W^{5+}$or $W^{5+} \longleftrightarrow W^{4+}$) [72], [73]. A combination of thickly packed polarons or large polarons and free carriers might exist at very high values of x.

5.2 Refractive Index, Film Density, and Electronic Polarizability

The density of bulk material or of a thin film can be calculated from refractive index data using the following well known expression [74], [75]

$$\frac{\rho_f}{\rho_b} = \frac{n_f^2 - 1}{n_f^2 + 2} \times \frac{n_b^2 + 2}{n_b^2 - 1}, \tag{19}$$

Where ρ_f is the average film density and ρ_b the bulk density of the material (in crystalline phase); $\boldsymbol{n}_f$ denotes the refractive index of the thin film and $\boldsymbol{n}_b$ the refractive index of bulk material (crystalline phase). Using the bulk values of n_b (of WO_3) as 2.5 and ρ_b (of WO_3) as 7.3 g cm^{-3}, we can transform Eq. (19) into

$$\rho_f = 11.47 \left[\frac{n_f^2 - 1}{n_f^2 + 2} \right]. \tag{20}$$

Moreover, the densities (ρ_f & ρ_b) and the porosities (f_p) of thin films are related by the equation [74], [75]

$$f_p = 1 - \rho_f / \rho_b \tag{21}$$

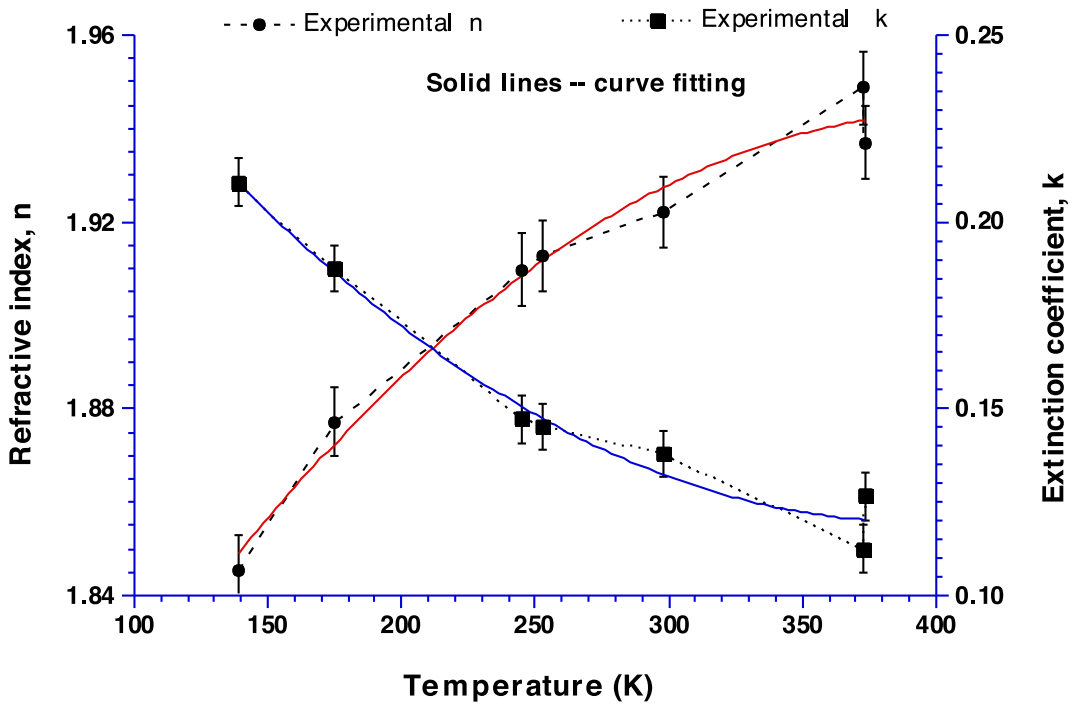

Fig. 7. Plot of (n, k) versus temperature, T, of $H_{0.15}WO_3$ thin film under vacuum in the range 130-297 K.

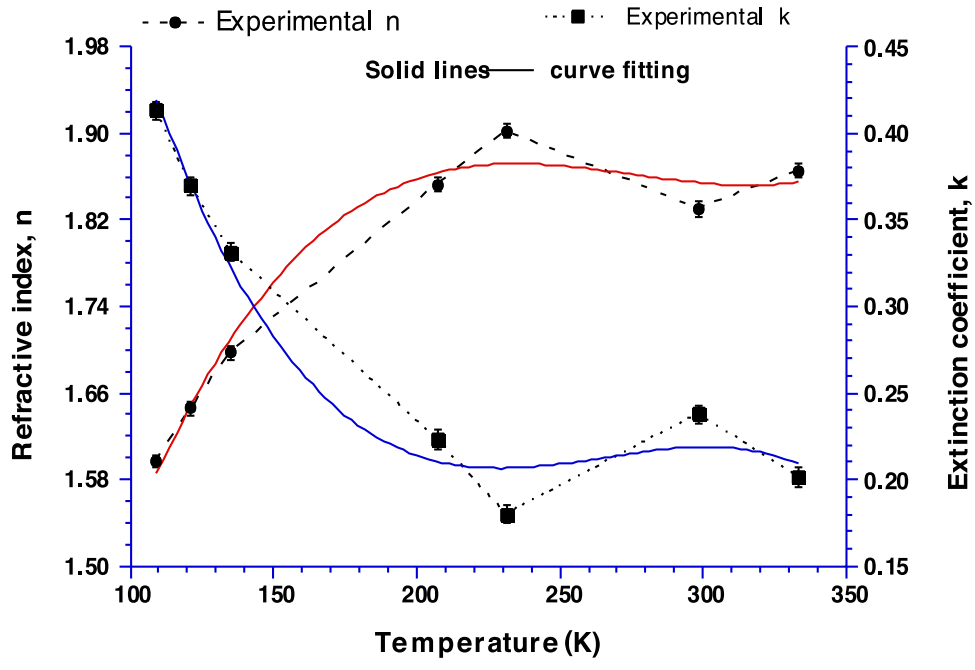

Fig. 8. Plot of (n, k) versus temperature, T, of $H_{0.26}WO_3$ thin film under vacuum in the range 120–297 K.

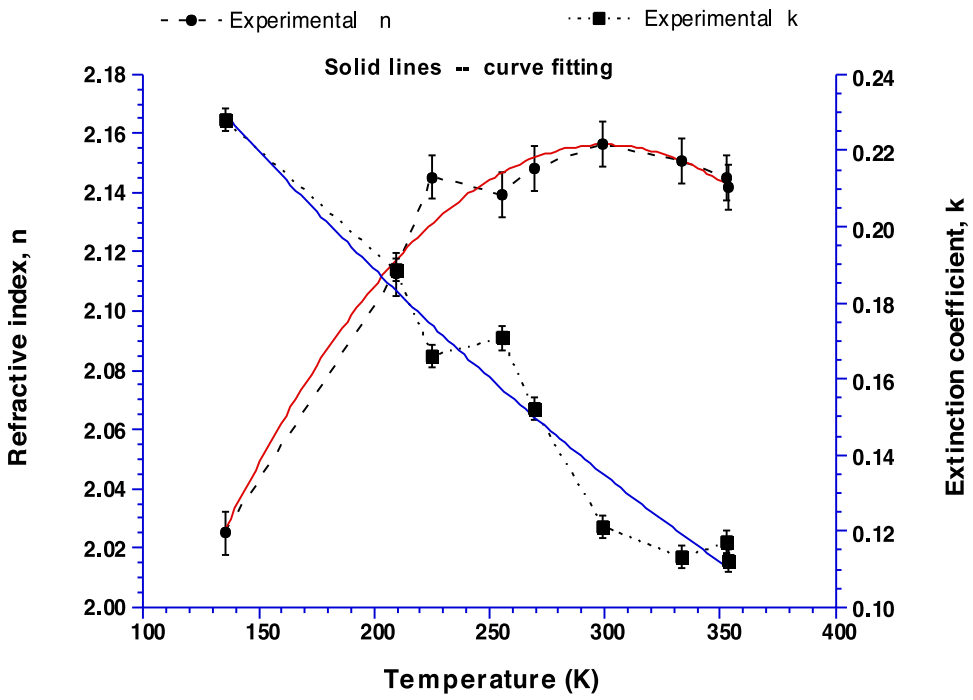

Fig. 9. Plot of (n, k) versus temperature, T, of $Li_{0.12}WO_3$ thin film under vacuum in the range 120–360 K.

The temperature dependent density and porosity data of WO_3, H_xWO_3, Li_xWO_3, and Na_xWO_3 thin films were calculated from Eqs. (20) and (21) using reported ellipsometric data on these films (Tables 1–4) and are displayed in Fig. 16 in the temperature range $295 \leq T \leq 373$ K. Similarly, from the data (Tables 6–11), the other plots of density & porosity are depicted in Figs. 17 & 18 in the temperature range $100 < T < 400$ K. The plots in Fig. 16 indicate that the density and porosity of WO_3 and M_xWO_3 bronzes change a little with the increase in temperature and this change is not more than 5% as compared to room temperature data. It is important to note that the advantage of heat-treatment is to reduce light scattering effects before utilizing of these sub-stoichiometric WO_3 films and its bronzes in electrochromic devices or in solid state microbatteries.

On the other hand, the plots in Figs. 17 and 18 show that the density and porosity of tungsten bronzes change a lot over the temperature range $100 < T < 300$ K due to porous nature of the bronze thin films.

In our case, the average size of crystallite is about 5 nm, which is very lower than the Bohr radius for WO_3 system (~13 nm), so we can assume the presence of weak quantum confinement [76], [77] associated with our WO_3 system which caused the higher band gaps in WO_3 thin films [46], [77]. So this system belongs to oxygen vacancies or defects [78], [79]. Moreover, the behaviour of optical constants (n, k) in the cooling process could be due to self-trapped charge carriers, known as small polaronic and bipolaronic species which will be explained fully in Section 5.4.

Next, we introduce the term polarizability of a material. The total polarizability of any material can be expressed as

$$\alpha_{tot} = \alpha_e + \alpha_i + \alpha_d, \tag{22}$$

Which is the sum of electronic (α_e), ionic (α_i), and dipolar (α_d) polarizabilities which determine the dynamical response of a bound system to external fields, and provide insight into a molecule's internal structure. It should be noted that when there is a permanent dipole moment in the material,

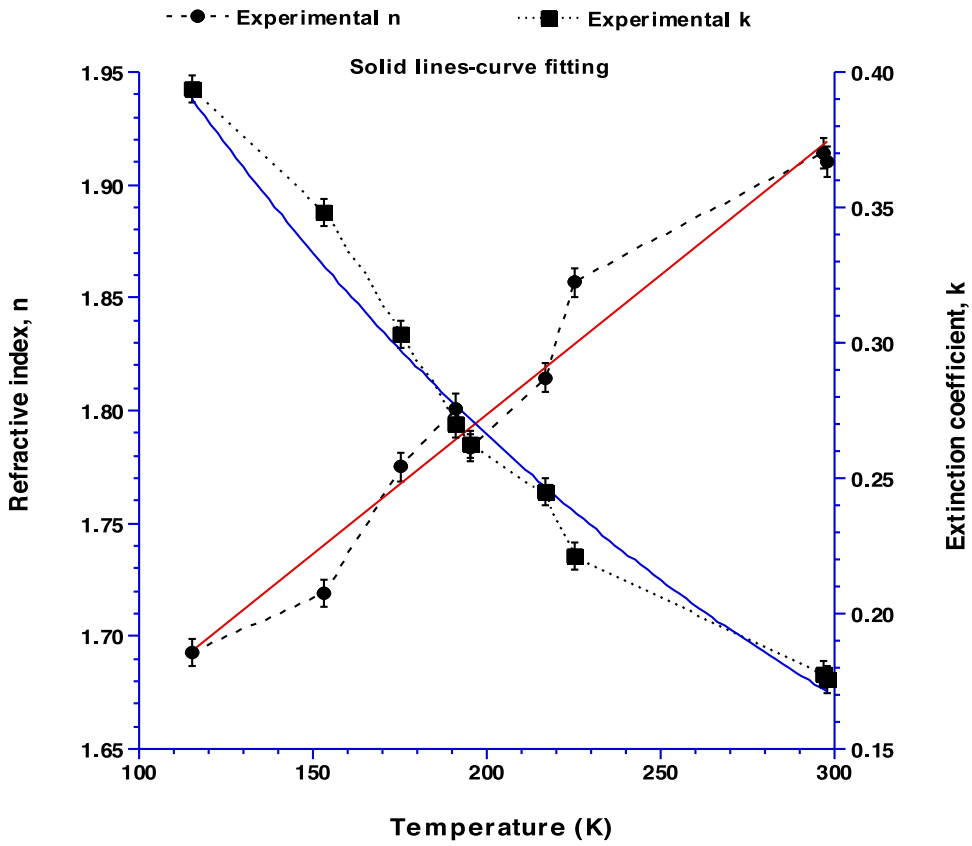

Fig. 10. Plot of (n, k) versus temperature, T, of $Li_{0.18}WO_3$ thin film under vacuum in the range 100–298 K.

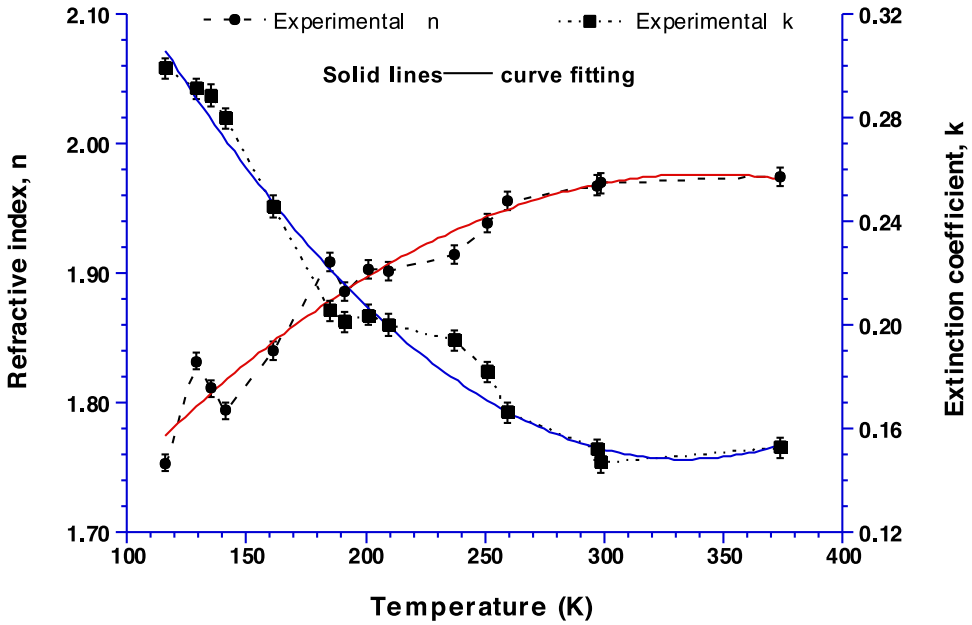

Fig. 11. Plot of (n, k) versus temperature, T, of $Na_{0.15}WO_3$ thin film under vacuum in the range 100–373 K.

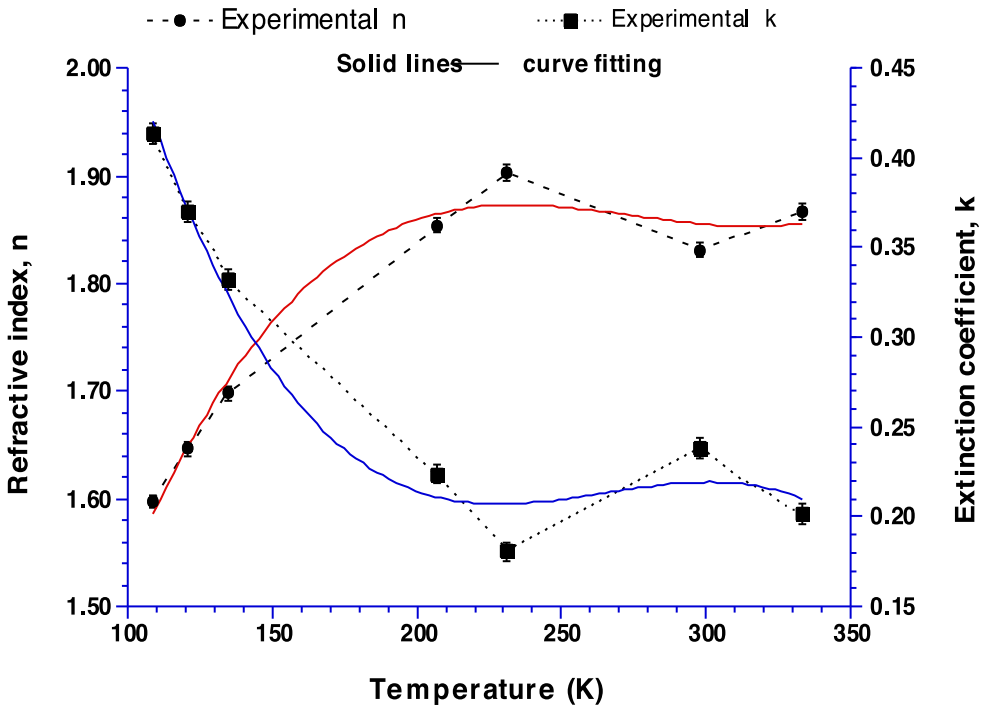

Fig. 12. Plot of (n, k) versus temperature, T, of $Na_{0.264}WO_3$ thin film under vacuum in the range 100–350 K.

TABLE 12

Error Analysis for the Vacuum-Ellipsometric Data on Tungsten Bronze Thin Films Over the Temperature Range 295 ≤ T ≤ 373 K (and within the Concentration Range, 0 < x ≤ 0.4)

Type of material	x	Thickness (μm)	δn	δk
WO_3	0.000	0.30	±0.00100	±0.00023
H_xWO_3	0.120	0.435	±0.00011	±0.00020
Li_xWO_3	0.313	0.29	±0.00018	±0.00046
Na_xWO_3	0.105	0.22	±0.00023	±0.00059

the material is called dipolar material. When an external field (like electric field, etc) is applied however, the molecules will begin to rotate to align the molecules with the field and this process of orientation of permanent dipole moments along the axis of the external field is called dipolar polarizability (α_d) or orientational polarizability. In the current situation, the external field is only visible range of solar spectrum and the strength of this field is not more than 10^5 V/cm, so the ionic polarizability (α_i) and dipolar polarizability of any solid material in the visible spectral range can be neglected. Since WO_3 thin film is a non–dipolar (ionic) material, so only the electronic polarizability (α_e) is present in the film (s) over the visible spectral range.

The refractive index (n_f) and film density (ρ_f) are related to electronic polarizability (α_e) through the famous Lorentz-Lorenz relation [80], [81],

$$\frac{n_f^2 - 1}{n_f^2 + 2} = \left[\frac{4\pi}{3} N_A \frac{\rho_f}{M}\right] \alpha_e. \tag{23}$$

Here, N_A is the Avogadro's number and M is the molecular weight of the material.

TABLE 13

Error Analysis for the Vacuum-Ellipsometric Data on Tungsten Bronze Thin Films Over the Temperature Range $100 \leq T \leq 295$ K (and within the Concentration Range, $0 < x \leq 0.4$)

Type of material	x	Thickness (μm)	δn	δk
WO_3	0.00	0.26	±0.00150	±0.00020
H_xWO_3	0.26	0.215	±0.00225	±0.00180
Li_xWO_3	0.18	0.24	±0.00635	±0.00138
Na_xWO_3	0.15	0.20	±0.00518	±0.00164

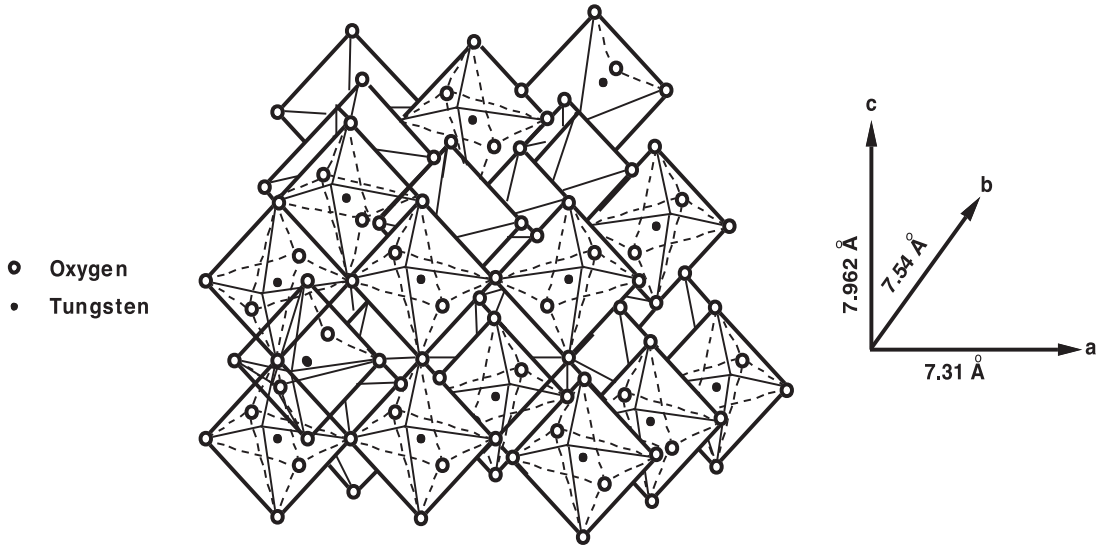

Fig. 13. Model of monoclinic (ReO_3 type) structure of WO_3 at room temperature.

Inserting the values of $N_A = 6.023 \times x10^{23}$ mol^{-1} and $M = 231.85$ g mol^{-1} into Eq. (23), the expression for electronic polarizability can be reshaped as

$$\alpha_e = 9.194 \times \frac{n_f^2 - 1}{n_f^2 + 2} \times 1/\rho_f. \tag{24}$$

The electronic polarizabilities of reported WO_3, H_xWO_3, Li_xWO_3, and Na_xWO_3 thin films were calculated from Eq. (24) by the help of refractive index (n_f) data (Tables 1 to 11) and from the film density (ρ_f) data using Eq. (20). The average electronic polarizability of WO_3 thin films as calculated from Eq. (24) at room temperature is found to be 8.02×10^{-24} cm^3. Plots of the measured electronic polarizabilities along with refractive indices versus temperature are represented in Figs. 19–21. It is very obvious from these plots that the values of electronic polarizability (or depolarization coefficients) of WO_3 thin films change very little over the whole heating and cooling process. This kind of behaviour is characteristic for the materials for which the temperature dependence of the optical indices is associated with thermal expansion [82].

It is clear from Figs. 20 and 21 that further decrease in the values of n (refractive index) due to temperature treatment regarding reported bronzes (H_xWO_3, Li_xWO_3, Na_xWO_3) are due to slight decrease in the electronic polarizability (from 8.020 to 8.003×10^{-24} cm^3), and that change in the polarizability is due to increase in the amorphousness in bronzes over the temperature range 100–373 K. It should be noted that a higher degree of crystallinity produced in WO_3 thin films at temperature higher than 673 K could give rise to a higher electronic polarizability.

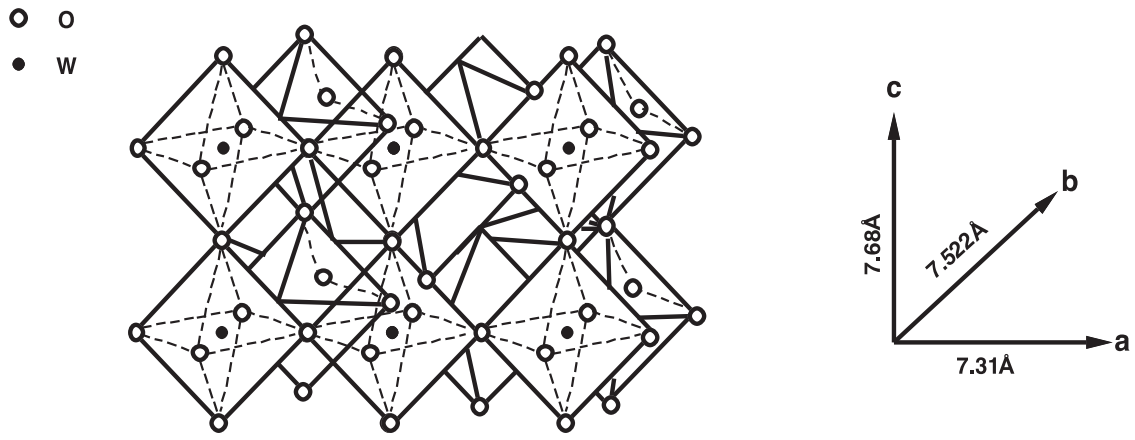

Fig. 14. Model of triclinic (ReO_3 type) structure of WO_3.

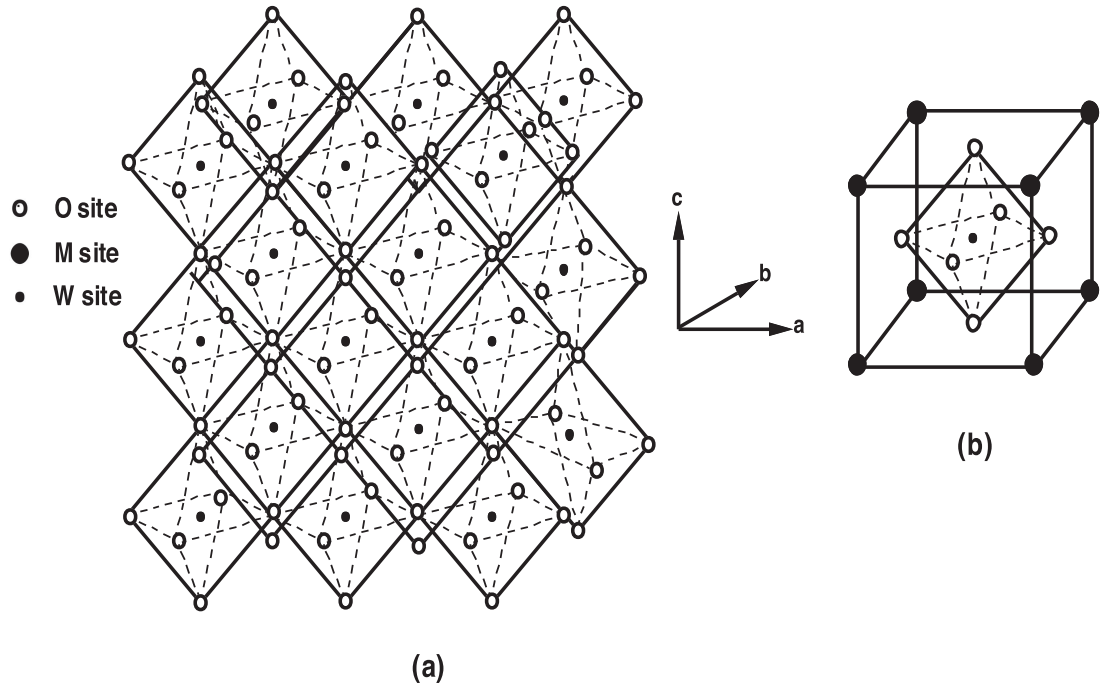

Fig. 15. (a) Crystal model for the perovskite related structure of M_xWO_3 ($M = Li^+, Na^+$). (b) Perovskite unit cell of cubic M_xWO_3 ($x \leq 1$).

5.3 Thermo-Optic Coefficients and Interpretations

In the first step, thermo optic coefficients (dn/dT and dk/dT) of WO_3, H_xWO_3, Li_xWO_3, and Na_xWO_3 for the heating cycles over the temperature range 295–373 K are measured from Figs. 2–5. Full details of the thermo optic coefficients (TOCs) can be obtained from Tables 1–4. We have also developed the mathematical formulations for the concentration and temperature dependent refractive index data and for the associated thermo optic coefficients. The following are the mathematical equations which fit to the reported temperature dependent n and k data.

$$n(T) = n_0 + A_n x + B_n (T - T_0), \tag{25}$$

$$k(T) = k_0 + C_k x + D_k (T - T_0). \tag{26}$$

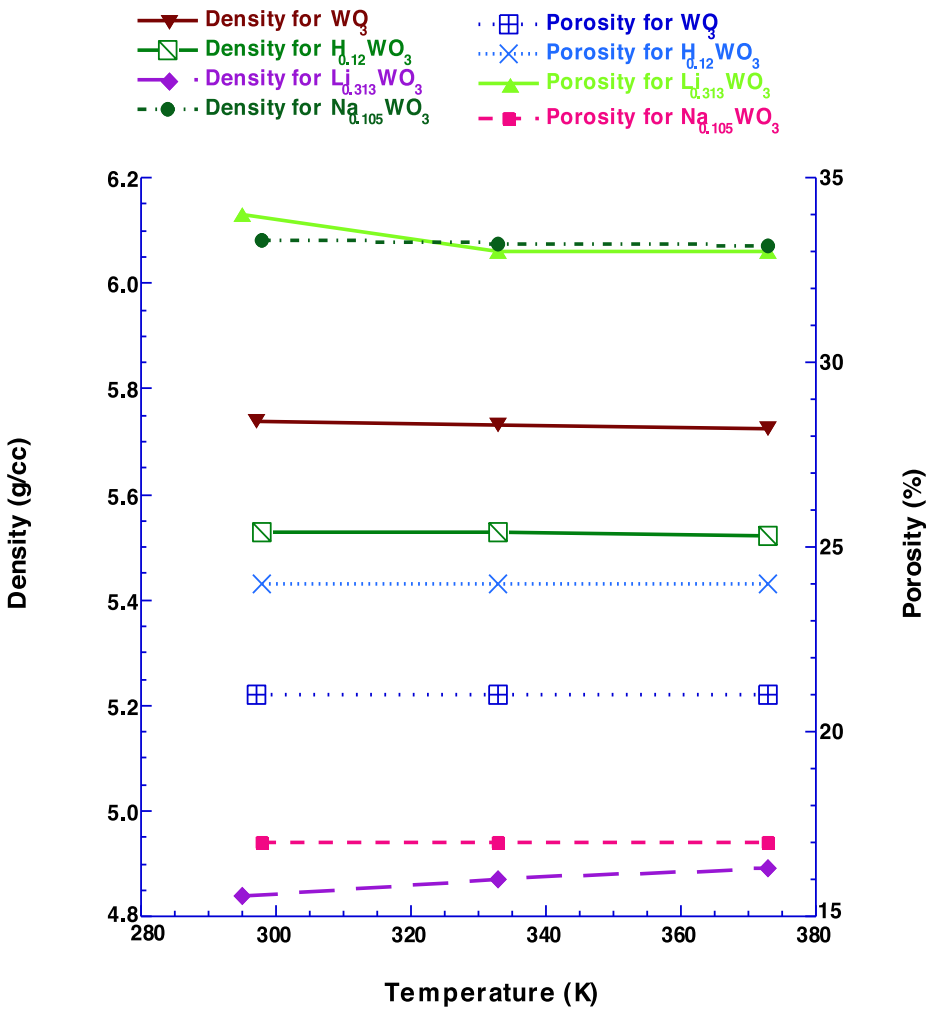

Fig. 16. Plots of density and porosity versus temperature, T, of WO_3, $H_{0.12}WO_3$, $Li_{0.313}WO_3$, and $Na_{0.105}WO_3$ thin films in the range 295–373 K.

In Eq. (25), n_0 and T_0 are initial values (room temperature values) and n and T are any selected (or final) values of refractive index and temperature. A_n is a constant associated with the concentration (x), and B_n is taken as an average value of dn/dT associated with the temperature dependent n-data of any reported tungsten bronze at a particular x-value with some $\pm$ standard deviation. Similarly, in Eq. (26), k_0 and T_0 are initial values (room temperature values) and k and T are any selected (or final) values of extinction coefficient and temperature. C_k is a constant associated with the concentration (x), and D_k is taken as an average value of dk/dT associated with the temperature dependent k-data of any reported tungsten bronze at a particular x-value with some $\pm$ standard deviation.

In the case of WO_3, the values of TOCs (dn/dT and dk/dT) from Fig. 2 (and verified from Table 1) can be fitted to Eqs. (25) and (26) as

$$n(T) = 2.0018 + B_n(T - T_0), \tag{27}$$

where x = 0 and $B_n = [-5.33 \pm 0.065] \times 10^{-5} K^{-1}$, and

$$k(T) = 0.00015 + C_k x + D_k(T - T_0), \tag{28}$$

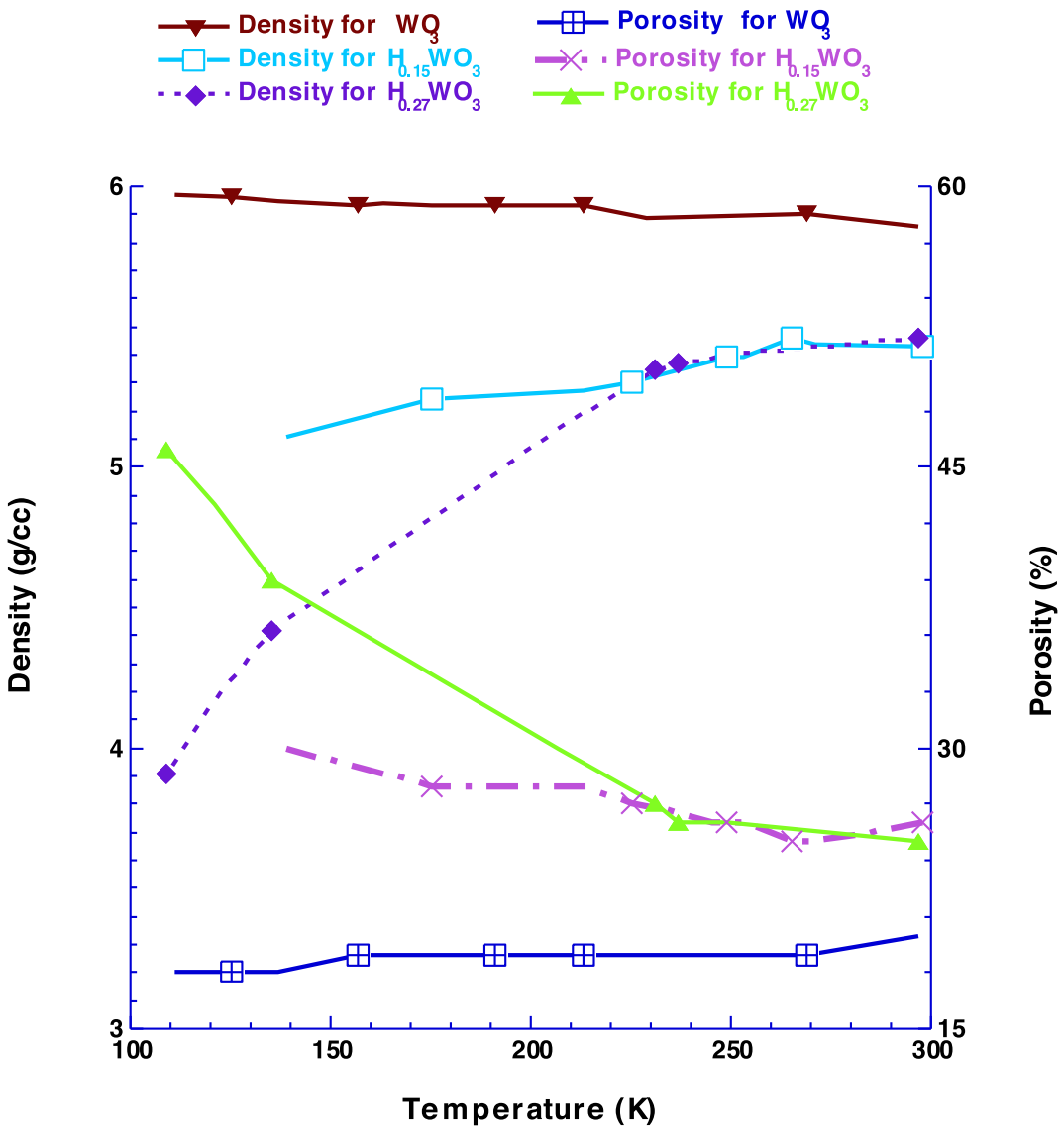

Fig. 17. Plots of density and porosity versus temperature, T, of WO_3, $H_{0.15}WO_3$, and $H_{0.27}WO_3$ thin films in the range 100–300–K.

where x = 0 and $D_k = [3.49 \pm 0.99] \times 10^{-6} K^{-1}$.

The overall accuracy in fitting the numerical relations (27) & (28) to the reported data for WO_3 thin film is correct to within ±3%.

The values of TOCs from Fig. 3 (or Table 2) regarding $H_{0.12}WO_3$ can be fitted to Eqs. (25) and (26) as

$$n(T) = 1.9477 + A_n x + B_n (T - T_0), \tag{29}$$

where x = 0.12, $A_n = 3.85 \times 10^{-4}$ and $B_n = [3.401 \pm 3.27] \times 10^{-5} K^{-1}$, and

$$k(T) = 0.11367 + C_k x + D_k (T - T_0), \tag{30}$$

where x = 0.12, $C_k = 3.80 \times 10^{-5}$ and $D_k = [-6.31 \pm 3.71] \times 10^{-5} K^{-1}$.

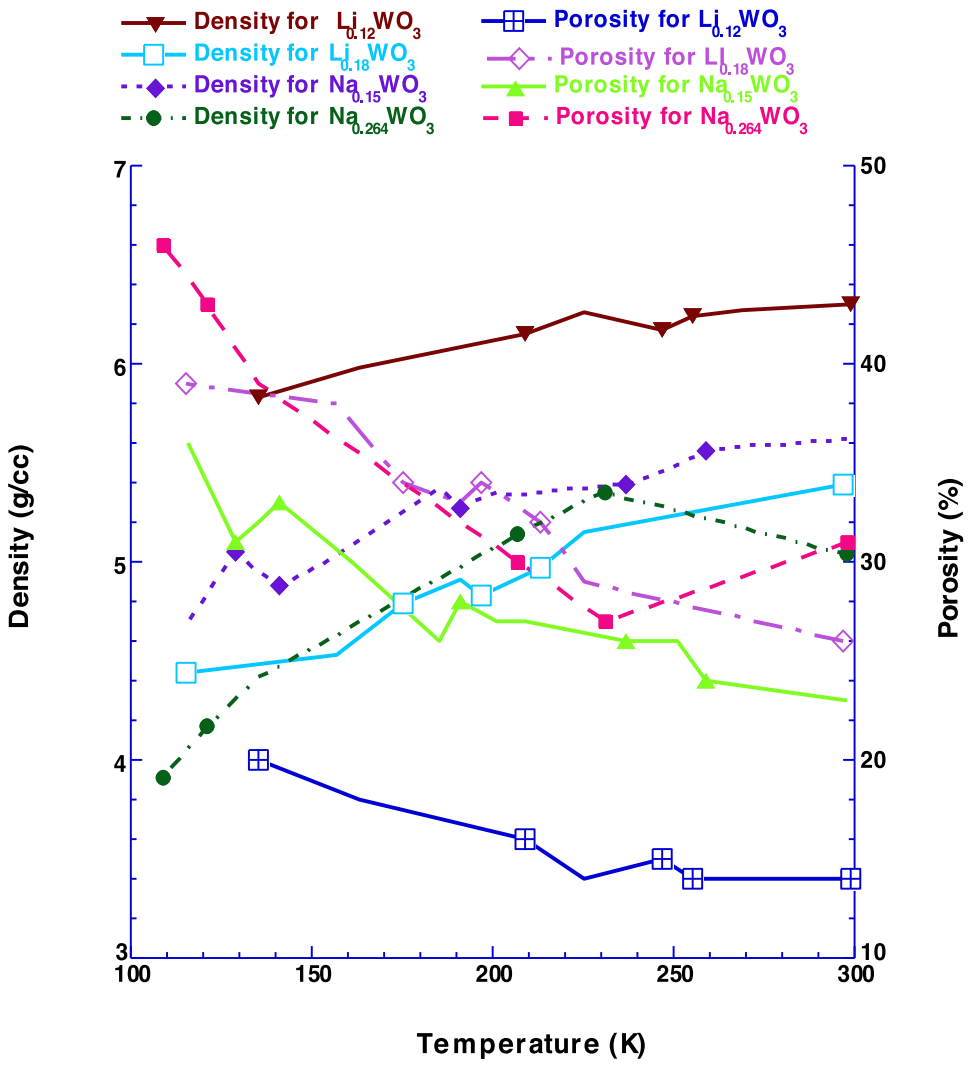

Fig. 18. Plots of density and porosity versus temperature, T, of $Li_{0.12}WO_3$, $Li_{0.18}WO_3$, $Na_{0.15}WO_3$, and $Na_{0.264}WO_3$ thin films in the range 100–300 K.

The values of TOCs from Fig. 4 (or Table 3) regarding $Li_{0.313}WO_3$ can be fitted to Eqs. (25) and (26) as

$$n(T) = 1.7853 + A_n x + B_n (T - T_0), \tag{31}$$

where x = 0.313, $A_n = 3.85 \times 10^{-4}$ and $B_n = [1.63 \pm 0.14] \times 10^{-4} K^{-1}$, and

$$k(T) = 0.11690 + C_k x + D_k (T - T_0), \tag{32}$$

where x = 0.313, $C_k = 3.80 \times 10^{-5}$ and $D_k = [-4.634 \pm 2.37] \times 10^{-5} K^{-1}$.

The numerical relations (29) to (32) are fitted well to the reported data for $H_{0.12}WO_3$ and $Li_{0.313}WO_3$ with an accuracy of ±7%.

The respective values of TOCs from Fig. 5 (and verified from Table 4) regarding $Na_{0.105}WO_3$ vary from -3.733×10^{-5} K^{-1} to 1.333×10^{-6} K^{-1} and -3.12×10^{-5} K^{-1} to 1.333×10^{-6} K^{-1} in the range 298–373 K; but, it is important to note that there is no mathematical formulation possible due to anomalous dispersion in the data. Nonetheless, the detailed graphical behaviour of thermo

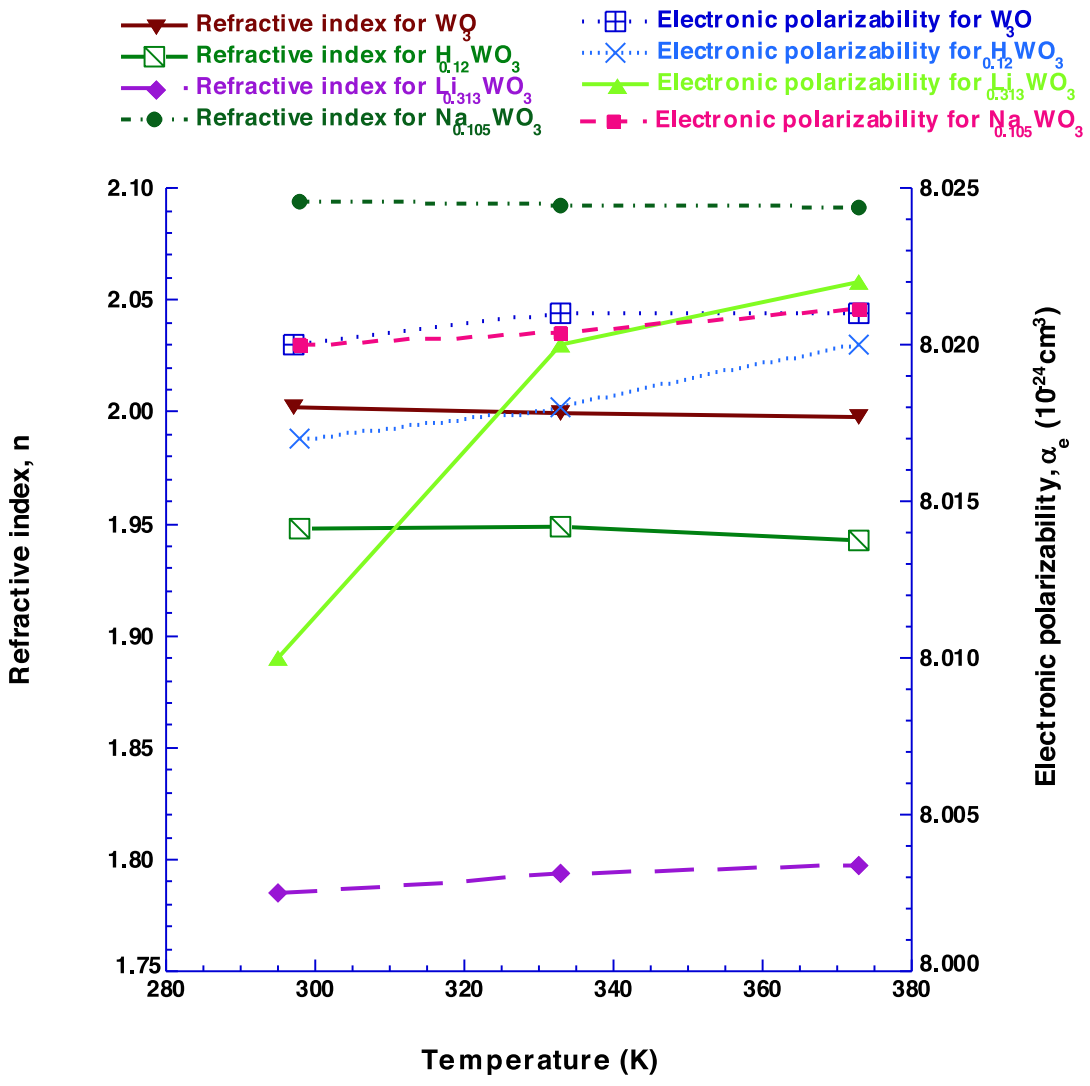

Fig. 19. Plots of refractive index and electronic polarizability versus temperature, T, of WO_3, $H_{0.12}WO_3$, $Li_{0.313}WO_3$, and $Na_{0.105}WO_3$ thin films in the range 295–373 K.

optic coefficients for WO_3, $H_{0.12}WO_3$, $Li_{0.313}WO_3$ and $Na_{0.105}WO_3$ (Figs. 2–5) can also be verified by experimental data as given in Tables 1–4.

In the second step, we have measured the thermo optic coefficients of WO_3, H_xWO_3, Li_xWO_3, and Na_xWO_3 thin films from Figs. 6–12 (or from Tables 5–11) for the cooling cycles over the temperature range 100–300 K.

In the case of WO_3, the values of TOCs from Fig. 6 (or from Table 5) can be fitted to Eqs. (25) and (26) as

$$n(T) = 2.0342 + B_n(T - T_0), \tag{33}$$

where x = 0 and $B_n = [-1.41 \pm 0.164] \times 10^{-4} K^{-1}$, and

$$k(T) = 0.00801 + C_k x + D_k(T - T_0), \tag{34}$$

where x = 0 and $D_k = [3.113 \pm 1.13] \times 10^{-5} K^{-1}$.

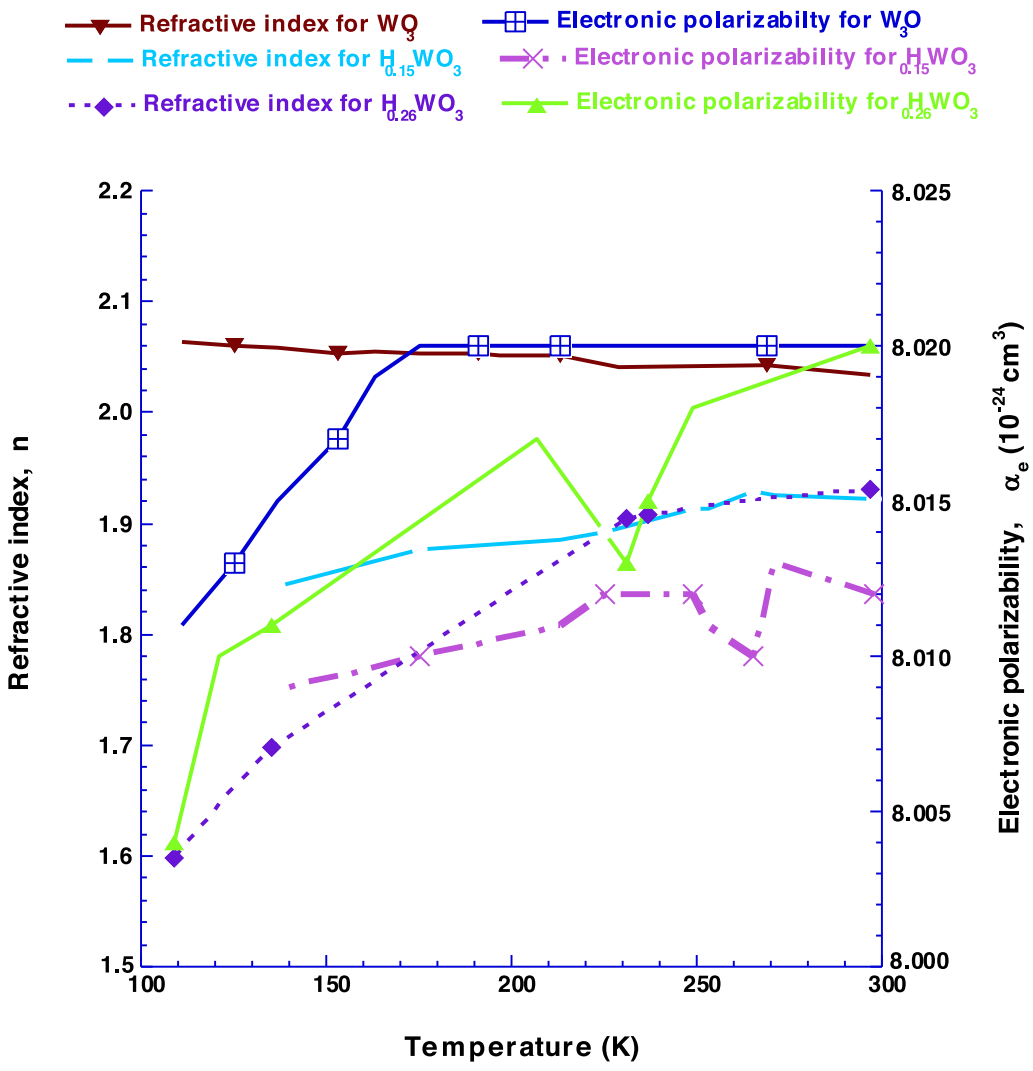

Fig. 20. Plots of refractive index and electronic polarizability versus temperature, T, of WO_3, $H_{0.15}WO_3$, and $H_{0.26}WO_3$ thin films in the range 100–300 K.

The accuracy in fitting the numerical relations (33) & (34) to the reported experimental data for WO_3 thin film is correct to within ±2%.

The values of TOCs from Fig. 7 (or from Table 6) regarding $H_{0.15}WO_3$ can be modelled as

$$n(T) = 1.9221 + A_n x + B_n (T - T_0), \tag{35}$$

where x = 0.15, $A_n = 3.85 \times 10^{-4}$ and $B_n = [5.54 \pm 0.724] \times 10^{-4} K^{-1}$, and

$$k(T) = 0.13790 + C_k x + D_k (T - T_0), \tag{36}$$

where x = 0.15, $C_k = 3.80 \times 10^{-5}$ and $D_k = [-5.342 \pm 0.767] \times 10^{-4} K^{-1}$.

The values of TOCs from Fig. 8 (or from Table 7) regarding $H_{0.26}WO_3$ can be fitted as

$$n(T) = 1.9311 + A_n x + B_n (T - T_0), \tag{37}$$

where x = 0.26, $A_n = 3.85 \times 10^{-4}$ and $B_n = [15.00 \pm 3.0] \times 10^{-4} K^{-1}$, and

$$k(T) = 0.16231 + C_k x + D_k (T - T_0), \tag{38}$$

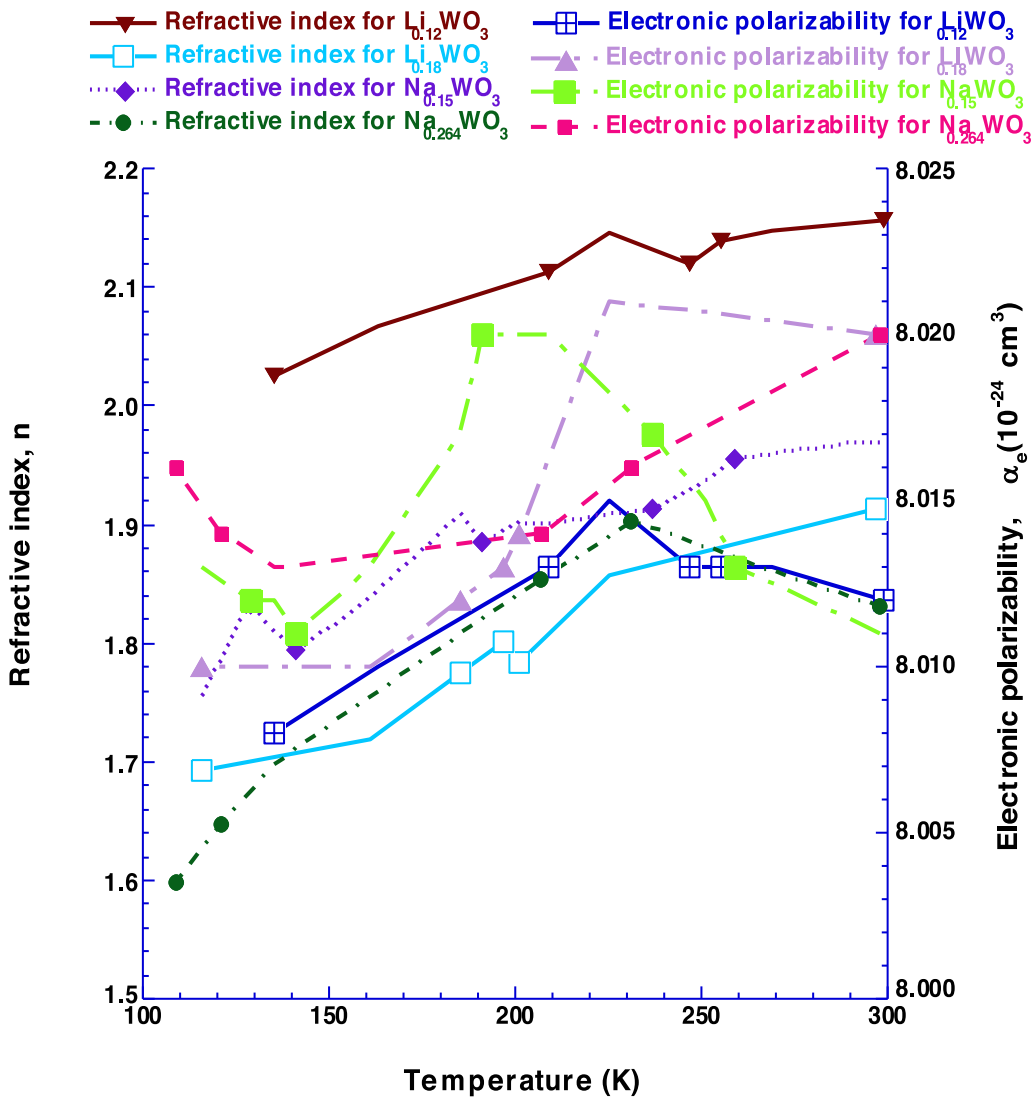

Fig. 21. Plots of refractive index and electronic polarizability versus temperature, T, of $Li_{0.12}WO_3$, $Li_{0.18}WO_3$, $Na_{0.15}WO_3$, and $Na_{0.264}WO_3$ thin films in the range 100–300 K.

where x = 0.26, $C_k = 3.80 \times 10^{-5}$ and $D_k = [-11.36 \pm 2.03] \times 10^{-4} K^{-1}$.

The accuracy in fitting the numerical relations (35) & (38) [for $H_{0.15}WO_3$ and $H_{0.26}WO_3$] is correct to within ±6%.

Similarly, the values of TOCs from Fig. 9 (or from Table 8) regarding $Li_{0.12}WO_3$ can be fitted as

$$n(T) = 2.1565 + A_n x + B_n (T - T_0), \tag{39}$$

where x = 0.26, $A_n = 3.85 \times 10^{-4}$ and $B_n = [7.68 \pm 0.37] \times 10^{-4} K^{-1}$, and

$$k(T) = 0.12149 + C_k x + D_k (T - T_0), \tag{40}$$

where x = 0.12, $C_k = 3.80 \times 10^{-5}$ and $D_k = [-6.90 \pm 0.35] \times 10^{-4} K^{-1}$.

Next, the values of dn/dT and dk/dT from Fig. 10 (or from Table 9) regarding $Li_{0.18}WO_3$ can be modelled as

$$n(T) = 1.9138 + A_n x + B_n (T - T_0), \tag{41}$$

where x = 0.18, $A_n = 3.85 \times 10^{-4}$ and $B_n = [11.7 \pm 0.30] \times 10^{-4} K^{-1}$, and

$$k(T) = 0.17735 + C_k x + D_k (T - T_0), \tag{42}$$

where x = 0.12, $C_k = 3.80 \times 10^{-5}$ and $D_k = [-11.87 \pm 0.02] \times 10^{-4} K^{-1}$.

The accuracy in fitting the numerical relations (39) to (42) [for $Li_{0.12}WO_3$ and $Li_{0.18}WO_3$] is correct to within ±5%.

In the case of $Na_{0.15}WO3$, the data of TOCs from Fig. 11 (or from Table 10) can be modelled as

$$n(T) = 1.9694 + A_n x + B_n (T - T_0), \tag{43}$$

where x = 0.15, $A_n = 3.85 \times 10^{-4}$ and $B_n = [9.904 \pm 1.9010] \times 10^{-4} K^{-1}$, and

$$k(T) = 0.14688 + C_k x + D_k (T - T_0), \tag{44}$$

where x = 0.15, $C_k = 3.80 \times 10^{-5}$ and $D_k = [-18.11 \pm 0.19] \times 10^{-4} K^{-1}$.

Fig. 12 (or from Table 11) gives the data of TOCs for $Na_{0.264}WO_3$ which can be modelled as

$$\boldsymbol{n(T) = 1.8308 + A_n x + B_n (T - T_0)}, \tag{45}$$

where x = 0.264, $A_n = 3.85 \times 10^{-4}$ and $B_n = [11.85 \pm 0.48] \times 10^{-4} K^{-1}$, and

$$k(T) = 0.23828 + C_k x + D_k (T - T_0), \tag{46}$$

where x = 0.264, $C_k = 3.80 \times 10^{-5}$ and $D_k = [-9.064 \pm 0.215] \times 10^{-4} K^{-1}$.

The numerical relations (43) to (46) are fitted well to the reported data for $Na_{0.15}WO_3$ and $Na_{0.264}WO_3$ with an accuracy of ±10%. The detailed graphical behaviour of thermo optic coefficients for WO_3, H_xWO_3 (x = 0.15, 0.26), Li_xWO_3 (x = 0.12, 0.18), and Na_xWO_3 (x = 0.15, 0.264) can be observed in Figs. 6–12. The data of these figures can also be verified from Tables 1 to 11.

The reported data on TOCs and the electronic polarizability (α_e) shows that there is very minute change in the TOCs due to a small change in the electronic polarizability in the temperature range $295-373\ K$. It is clearly visible that after heating in the above temperature range, the new values of optical constants of WO_3 and its bronzes are very close to their initial values. This means that the thermal treatment in the temperature range from 295 to 373 K is reversible. In a reversible process, we should obtain closed thermal hysteresis for the heating (or cooling) cycles of the films. So, the values of n and k, as depicted in Figs. 2–5 form approximate closed loops. This behaviour is characteristic for the materials for which the temperature dependence of the optical indices is associated with thermal expansion.

In terms of electrochromic properties and other technical applications, the tungsten bronze films heated up to 373 K give very good electrochromic response, as is evident from reversibility test plots in Figs. 2–5. It is also a universal fact that amorphous phase has larger charge density than a crystalline phase, because ion carriers move in amorphous phase faster and more easily than in crystalline phase [83]–[85].

As-grown film is always an amorphous or microcrystalline, it can transform to monoclinic/orthorhombic phase upon annealing at around 673 K [86], [87]. After annealing, the high porosity structure of WO_3 might reduce to more compact film, but the process of hydrogen, lithium or sodium ion intercalation and de-intercalation might become very difficult to occur in the newly crystallized phase of WO_3 thin film resulting in a lot of reduction in the colouration efficiency.

For the cooling cycles (Figs. 6–12), the hysteresis loops are not closed for the investigated ellipsometric data. This means that the thermal treatment in the temperature range 100 to 300 K is irreversible. Nonetheless, thermo-optical coefficients (dn/dT) relating to H_xWO_3(x = 0.15, 0.26), Li_xWO_3 (x = 0.12, 0.18), and Na_xWO_3 (x = 0.15, 0.264) as determined from Figs. 6–12 (or from Tables 5 to 11) are found to be positive in the visible part of spectral range, and have values in the range from 4.811×10^{-4} K^{-1} to 18.03×10^{-4} K^{-1} over the temperature range 100–373 K. Similarly, dk/dT values for the bronzes determined from Figs. 6–12 (or from Tables 5 to 11) are all negative and range from -4.56×10^{-4} K^{-1} to -18.02×10^{-4} K^{-1} over the same temperature

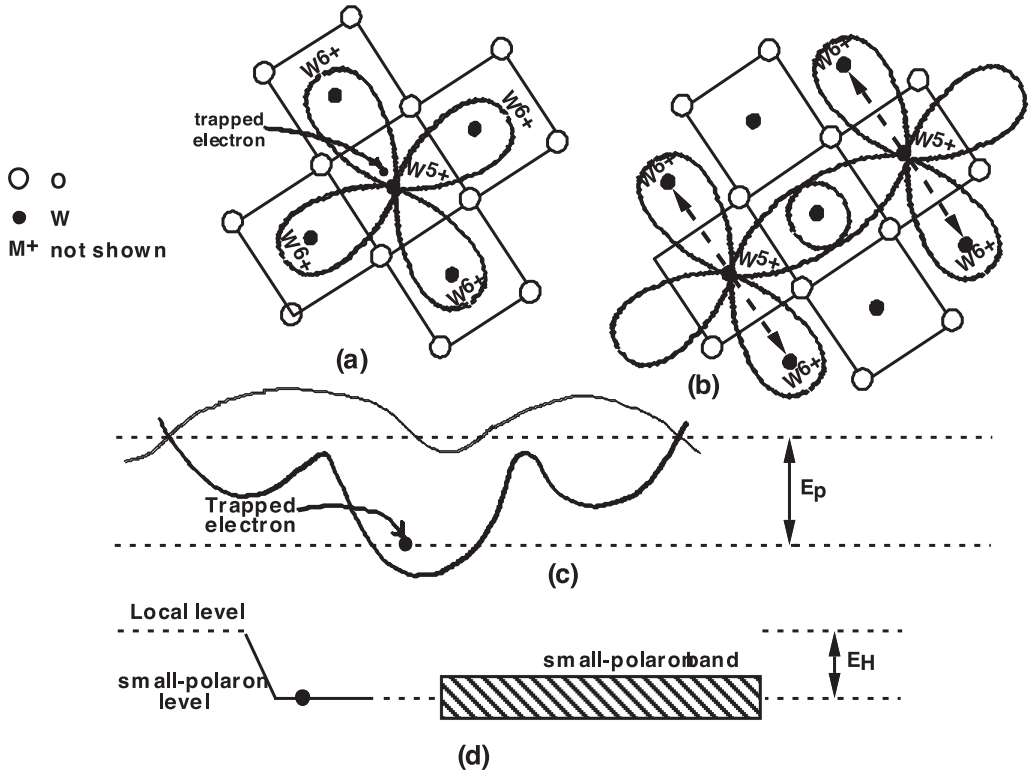

Fig. 22. An outline of a single polaron, (a), and a bipolaron, (b) in n type lattice structure of M_xWO_3 (H^+, Li^+, Na^+) bronzes; a sketch of a potential well for a trapped electron, (c), and a view of a small-polaron band, (d).

range. It is important to note that these small changes in TOCs are due to small changes in the values of electronic polarizability, as identified in Figs. 20 and 21.

The changes in (n, k) during cooling cycles, can be related to increased randomization in inter-nuclear distances and chemical bondings [71], [88]. The low temperature experimental data also verify that when the samples return to room temperature, they exhibit only meagre modifications in their morphology. In other words, the shifts in k values may cause a small increase in the total crystal energy due to some distortions but the end-product never change into crystallographic stable phases [58], [89].

There is also an anomalous behaviour for some optical data, over a small temperature range (Figs. 10–12), but this behaviour may be due to the presence of dangling bonds in the films. It should be noted that there is no sign of sharp onsets of k values, nor of temperature independent behaviour of k values, indicating absence of metal-semiconductor transitions in the aforesaid low temperature range.

5.4 Polaronic and Bipolaronic Excitations and Hoppings

The changes in the colourations in tungsten bronzes, M_xWO_3 ($M = H^+$, Li^+, Na^+) at or above room temperature are caused because of polaronic excitations [Fig. 22(a)]. And for low temperatures, colouration changes may be due to excitations having bipolaronic ground states [Fig. 22(b)]. X-ray photoelectron spectroscopy (XPS) results [90], [91] prove that the hydrogen, lithium or sodium insertion is accompanied by a two-step reduction of tungsten. In the first step W^{6+} is reduced to W^{5+}, and in the second step W^{4+} is formed in addition, which suggests that the presence of W^{4+} is essential for the colouration of nano- crystalline or microcrystalline WO_3 thin films.

Bipolaron hopping needs more than twice the hopping energy (E_H) of single polaron for any optical (or electrical) transition. This is perhaps due to more relaxation time required in the case of bipolaronic mechanism. The predominant optical (or electrical) conduction near the fermi level may take place either via hopping of the polarons or bipolarons {see Fig. 22 (a), (b), (c), (d)}.

Hopping mechanism may occur when the concentration of sites is high enough to allow a non-negligible overlap of the individual wave functions. Within the band gap, the following conditions [90] are implied for non-adiabatic hoppings, i.e.,

$$J_{W_i - W_i} < 4E_H, \tag{47}$$

and

$$J_{W_i - W_i} < \left(\frac{E_H K_B T}{\pi}\right)^{1/4} (h\nu_{L_o})^{1/2}. \tag{48}$$

Where J is the resonance transition integral between nearest neighbours (W_i-W_i), k_B be the Boltzmann constant, and $\mathbf{h\nu_{Lo}}$ signifies longitudinal optical phonon energy. At higher temperatures, the condition becomes

$$\frac{\mathbf{K_B T}}{\mathbf{h\nu_{L_o}}} \gg \mathbf{1}, \tag{49}$$

where longitudinal optical mode ($\boldsymbol{\nu_{Lo}}$) is at the Brillouin zero wave vector. In Fig. 22[(c), (d)], E_p and E_H are the polaron binding energy and the thermal hopping energy of a polaron, respectively, and are connected by a relation [29], [91]

$$E_p = 2E_H, \tag{50}$$

which holds very well for non-adiabatic hopping with J $\sim$ 0. Thermal hopping energy, E_H is related to a coupling constant, γ by the relation [90], [92]

$$\frac{\gamma}{2} = 20 \times \frac{E_H}{h\nu_{L\,o}}, \tag{51}$$

where γ is also related to E_D and m_p by the expressions [90], [91]

$$\frac{\gamma}{2} = \frac{E_D}{h\nu_{L\,o}}, \tag{52}$$

and

$$\gamma = 2.66\left(\frac{m_p}{m_e^*}\right)^{1/4}. \tag{53}$$

Where E_D is the deformation energy of the polaron; $m_e{}^*$ be the effective electronic mass, and m_p be the polaronic effective mass. A hopping process was observed by the broadening of the W^{5+}species using electron spin resonance (ESR) signals [29], [52], [93], Electron spectroscopy for chemical analysis (ESCA) experiments [53], [94], [95], and X-ray photoelectron spectroscopy (XPS) studies [50], [96].

Bipolaronic and single polaronic excitations and transitions from one site to the nearest neighbour site in tungsten bronze thin films are better illustrated by the configurational coordinate model, as shown in Fig. 23. Irradiation of tungsten bronze with light energy, hν, causes bipolarons or single polarons to hop from their initial state (Q_A) to the nearest minimum potential energy state (Q_B). For bipolarons, the hopping thermal energy, $E_h{}^{bi}$ is related to the optical transfer energy, hν by the expression [91], [97], [98]

$$4E_H^{bi} = h\gamma. \tag{54}$$

A similar expression can also be given for single polarons, E_h^{si} for non-adiabatic hoppings. Further, $\boldsymbol{E_H^{bi}}$ is related to $\boldsymbol{E_H^{si}}$ by an inequality [71], [90], [92]

$$E_H^{bi} > < 2E_H^{si}, \tag{55}$$

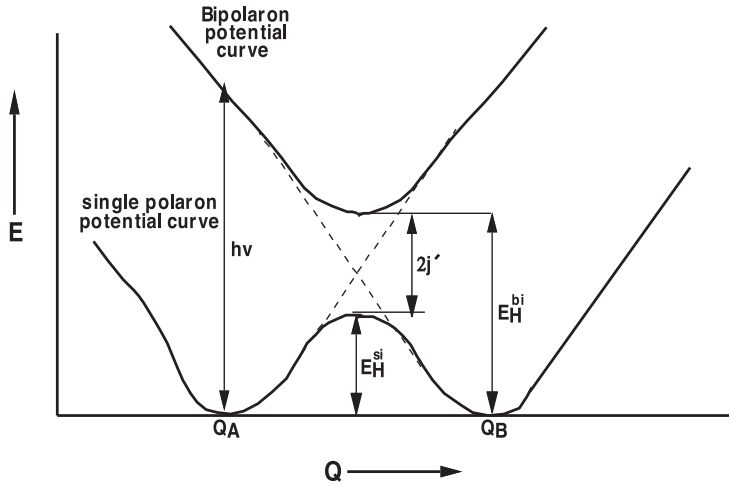

Fig. 23. Sketch for configurational co-ordinate model for a bipolaon and a small polaron, and illustrations for their binding energies.

with $<$ as lower bound and $>$ as upper bound stability conditions for bipolarons. $E_h^{bi} - 2E_h^{si}$ gives the difference between the bipolaronic ground state and its polaronic counterpart, which is equivalent to the thermal hopping energy to destabilize the excited bipolaronic wave function either around Q_A, or near Q_B site. The bipolaron can also be dissociated during irridation in the cooling process, and comes out of bipolaronic potential well in the form of two separate small polarons. These two polarons then hop over the potential curve, and eventually recombine in the single entity (bipolaron) at the final equilibrium state, Q_B. It is noticed that the mobility of bipolarons is much lower than that of the single polarons. As a result, k values (or conductivity) in the case of bipolaronic transitions are much lower than those of single polaron transitions. Dissociation and recombination energies, both are supposed to be positive because of the stability condition of bipolarons [90], [99].

Lower and higher temperature plots show that WO_3 has a lower dielectric constant (or n values) in the low temperature mode compared with the higher temperature mode. These results are in agreement with the proposed model that no heavy polarons exist in the lower temperature range, and that the associated binding energies increase due to bipolaron formation. From the low electron mobility data [98], [99], there are also signs of the existance of small polarons in WO_3, either at or above room temperature.

From the cold temperature plots (Figs. 6–12) of tungsten bronzes, the gradual decrease of n values with the temperature for any individual bronze is in accordance with the increase of bipolaron concentration. Stability of WO_3 film and its bronzes at low temperatures are due to the spatial arrangement of highly dense bipolaronic states situated somewhere in the crystallographic shear planes. Stability of these bronzes at room temperature are due to self-induced deep potential wells. As a result, H^+(Li^+ or Na^+) diffusion rates in such bronzes will be much slower than in crystalline bronzes. At very low temperature, the bipolarons were confined to two dimensional hopping within the coulomb gap. When the temperature increases towards room temperature, this is transformed to three-dimensional Mott variable range hopping. As the temperature goes on increasing, hopping between more spatial levels is possible, and more activation energy is needed for the conduction mechanism. The transition from hopping to free band conduction is possible at a temperature higher than 673 K.

6. Summary and Conclusions

M_xWO_3 ($M = H^+$, Li^+, Na^+) bronze thin films were deposited on unheated 7059 glass slides, and were found to be microcrystalline in nature at room temperature. The values of dn/dT for WO_3 thin films were found to be negative either in the heating cylcle (295–373 K) or in the cooling cycle

(100 $<$ T $<$ 300 K**)** and were found to be in the range of order of 10^{-4} K^{-1}, but the values of dk/dT were found to be positive in the heating or cooling cycle and were also of the order of 10^{-4} K^{-1}. On the other hand, dn/dT and dk/dT (TOCs) of tungsten bronzes were determined to be positive and negative in the heating and cooling cycles, respectively, but both were found to be in the order of 10^{-4} K^{-1}. In the heating cycles, TOCs for the tungsten bronzes change very little, but in cooling cycles, dn/dT varies from 4.811×10^{-4} K^{-1} to 18.03×10^{-4} K^{-1} and dk/dT changes from -4.54×10^{-4} K^{-1} to -18.02×10^{-4} K^{-1} over the temperature range 100–300 K.

Figs. 2 to 5 (heating cycles) show hysteresis loops of refractive index n and extinction coefficient k for WO_3 and for its bronzes which indicate that TOCs of bronzes over the temperature range 295–373 K are associated with the thermal expansion. Electrochromic characteristics are still excellent in the bronze thin films even after being heated up to 373 K. At temperature higher than 473 K, there could be an increase in α_e, but an irreversible disordering of the hydrogen, lithium or sodium atoms could occur. At this stage, there could be no simple numerical models which could govern the thermo optic coefficients simply because of anomalous dispersions expected to occur in the optical data.

For the cooling cycles (Fig. 6–12), the hysteresis loops are not closed for the investigated ellipsometric data. This means that the thermal treatment over the temperature range from 100 to 300 K is definitely irreversible. For cooling cycles, a sudden increase in dn/dT and a decrease in the values of dk/dT for tungsten bronzes is due to small decrease in the values of electronic polarizabilities (α_e) which were calculated in the range from 8.003 to $8.02 \times 10^{-24} cm^3$ over the temperature range from 100 to 300 K. This little decrease in α_e is due to creation of more amorphousness (or porosity) in the WO_3 structure during the cooling cycles.

The ellipsometric data was also interpreted in terms of polarons. Briefly**,** at very low temperatures, bipolarons are confined to two-dimensional hopping within the coulomb gap. When the temperature increases towards room temperature, these entities become single polarons and are transferred to three-dimensional Mott variable. A combination of thickly packed polarons and free carriers might exist at temperatures higher than 673 K.

Acknowledgment

The author would like to thanks the invaluable assistance provided by the technicians of the EEE laboratories. The contents of this paper reflect the view of the author, who is responsible for the facts and the accuracy of the data presented.

References

[1] C. G. Granqvist, "Electrochromism and smart window design," *Solid State Ionics*, vol. 53, pp. 479–489, 1992.
[2] A. Pawlicka, F. Sentanin, A. Firmino, J. G. Grote, F. Kajzar, and I. Rau, "Ionically conducting DNA-based membranes for electrochromic devices," *Synthetic Metals*, vol. 161/21-22, pp. 2329–2334, 2011.
[3] W. Yang, F. L. Runnersstrom, and D. J. Milliron, "Switching materials for smart windows," *Ann. Rev. Chem. Biomol. Eng.*, vol. 7, pp. 283–304, 2016.
[4] C. G. Granqvist, "Solar energy materials," *Adv. Mater.*, vol. 15/21, pp. 1789–1803, 2003.
[5] P. M. S. Monk, R. J. Mortimer, and D. R. Rosseinsky, *Electrochromism and Electrochromic Devices.*, New York, NY, USA: Cambridge Univ. Press, 2007.
[6] J. C. Hill and K. S. Choi, "Effect of electrolytes on the selectivity and stability of n-type WO_3 to electrodes for use in solar water oxidation," *J. Phys. Chem. C.*, vol. 116, pp. 7612–7620, 2012.
[7] M. Leidinger, J. Huotari, T. Sauerwald, J. Lappalainen, and A. Schutze, "Selective detection of Naphthalene with nanostructured WO_3 gas sensors prepared by pulsed laser deposition," *J. Sens. Syst.*, vol. 5, pp. 147–156, 2016.
[8] A. Hemberg *et al.*, "Effect of the thickness of reactively sputtered WO_3 submicron thin films used for NO_2 Detection," *Sens. Actuators B-Chem.*, vol. 171, pp. 18–24, 2012.
[9] B. T. Sone *et al.*, "Synthesis and structural characterization of tungsten trioxide nanoplatelet-containing thin films prepared by aqueous chemical growth," *Nanoplatelet-Containing Thin Films*, vol. 522, pp. 164–170, 2012.
[10] A. Granqvist, *Handbook of Inorganic Electrochromic Materials.* Amsterdam, The Netherlands: Elsevier Science, 1995.
[11] C. G. Granqvist, "Electrochromic tungsten oxide films: Review of progress 1993-1998," *Sol. Energy Mat. Sol. Cells*, vol. 60, pp. 201–262, 2000.
[12] M. B. Babu and K. V. Madhuri, "Structural, morphological and optical properties of electron beam evaporated WO_3 thin films," *J. Taibah Univ. Sci.*, vol. 11, pp. 1232–1237, 2017.

[13] A. Llordes, G. Garcia, J. M. Gazquez, and D. J. Tunable, "Near-infrared and visible light transmittance in nanocrystal-in-glass composites," *Nature*, vol. 500, pp. 323–332, 2013.
[14] C. G. Granqvist, "Electrochromics for smart windows: Oxide-based thin films and devices," *Thin Solid Films*, vol. 564, pp. 1–38, 2014.
[15] E. S. Lee and D. L. Dibartolomeo, "Application issues for large-area electrochromic windows in commercial buildings," *Sol. Energy Mater. Sol. Cells*, vol. 71, pp. 465–491, 2002.
[16] K. H. Krishna, O. M. Hussain, and C. M. Julien, "Electrochromic properties of nanocrystalline WO_3 thin films grown on flexible substrates by plasma-assisted evaporation technique," *Appl. Phys. A*, vol. 99, pp. 921–929, 2010.
[17] C. O. Avellaneda and L. O. S. Bulhoes, "Photochromic properties of WO_3:x (x = Ti, Nb, Ta and Zr) Thin films," *Solid State Ionics*, vol. 165, pp. 117–121, 2003.
[18] S. H. Lee *et al.*, "Gasochromic mechanism in a-WO_3 thin films based on Raman spectroscopic studies," *J. Appl. Phys.*, vol. 88, pp. 3076–3078, 2000.
[19] M. A. Gondal, A. Hameed, Z. H. Yamani, and A. Suwaiyan, "Laser induced photo-catalytic oxidation/splitting of water over α -Fe_2O_3, WO_3, TiO_2 and NiO catalysts: Activity comparison," *Chem. Phys. Letts.*, vol. 385, pp. 111–115, 2004.
[20] C. S. Vazquez *et al.*, "Photocatalysis: Evidence and effect of photogenerated charge transfer for enhanced photocatalysis in WO_3/TiO_2heterojunction films: A computation and experimental study," *Adv. Funct. Mater.*, vol. 27, 2017, Art. no. 1605413.
[21] M. Feng *et al.*, "Strong photoluminescence of nanostructured crystalline tungsten oxide thin films," *Appl. Phys. Lett.*, vol. 86, 2005, Art. no. 141901.
[22] M. A. Habib, "Electrochromism," Tech. Rep., GMR 70C8, General Motors Research Laboratories, Jun. 1990.
[23] A. L. Larsson and G. A. Niklasson, "Infrared emittance modulation of all thin film electrochromic devices," *Mater. Lett.*, vol. 58, pp. 2517–2520, 2004.
[24] M. C. Rao, "Structure and properties of WO_3 thin films for electrochromic device application," *J. Non-Oxide Glasses*, vol. 5, pp. 1–8, 2013.
[25] Y. A. Yang and J. N. Yao, "Microstructural properties of an electrochromic WO_3 thin films," *J. Phys. Chem. Solids*, vol. 61, pp. 647–650, 2000.
[26] G. Xie, J. Yu, X. Chen, and Y. Jiang, "Gas sensing characteristics of WO_3 vacuum deposited thin films," *Sens. Actuators B.*, vol. 123, pp. 909–914, 2007.
[27] A. Karuppasamy, "Electrochromism and photocatalysis in dendrite structured Ti: WO_3 thin films grown by sputtering," *Appl. Surf. Sci.*, vol. 359, pp. 841–846, 2015.
[28] K. Yananaka, "Degradation caused by substrate glass in WO_3 electrochromic devices," *J. Appl. Phys.*, vol. 54, pp. 1128–1132, 1983.
[29] T. Oi, "Electrochromic materials," *Ann. Rev. Mater. Sci.*, vol. 16, pp. 185–201, 1986.
[30] V. M. Ischuk, L. A. Kvichko, V. P. Seminozhenko, V. L. Sobolev, and N. A. Spiridonov, "Ferroelectric phase transitions in oxides of the persovskite family," *JETP Lett.*, vol. 49, pp. 389–391, 1989.
[31] R. Salchow and R. Liebmann, "Superconducting transition temperature for polar metals: Na_xWO_3," *Phy. B.*, vol. 107, pp. 523–524, 1981.
[32] C. G. Granqvist, "Electrochromic materials: Microstructure, electronic bands, and optical properties," *Appl. Phys. A.*, vol. 57, pp. 3–12, 1993.
[33] S. K. Deb, "Opportunities and challenges of electrochromic phenomenon in transition metal oxides," *Sol. Energy Mater. Sol. Cells*, vol. 25, pp. 327–338, 1992.
[34] T. Kamimori, J. Nagai, and M. Mizuhashi, "Electrochromic devices for transmissive and reflective light control," *Sol. Energy Mater.*, vol. 16, pp. 27–38, 1987.
[35] P. R. Somani and S. Radhakrishnan, "Electrochromic materials and devices: Present and future," *Mater. Chem. Phys.*, vol. 77, pp. 117–133, 2003.
[36] Z. Hussain, "Optical constants and electrochromic characteristics of M_xWO_3 bronzes," *Appl. Opt.*, vol. 57, pp. 5720–5732, 2018.
[37] Z. Hussain, "Optical constants and electrochromic characteristics of H_xMoO_3 and Li_xMoO_3 bronzes," *JOSA A.*, vol. 35, pp. 817–829, 2018.
[38] K. J. Patel, C. J. Panchal, V. A. Kheraj, and M. S. Desai, "Growth, structural, electrical and optical properties of the thermally evaporated tungsten trioxide (WO_3) thin films," *Mater. Chem. Phys.*, vol. 114, pp. 475–478, 2009.
[39] R. Sivakumar, K. Shanthakumari, A. Thaymanavan, M. Jayachandran, and C. Sanjeerviraja, "Colouration and bleaching mechanism of tungsten oxide thin films in different electrolytes," *Surf. Eng.*, vol. 23, pp. 373–379, 2007.
[40] C. Y. Kim and S. Park, "Electrochromic properties of WO_3 thin film with various heat-treatment temperature," *Asian J. Chem.*, vol. 25, pp. 5874–5878, 2013.
[41] Z. Hussain, "Vacuum-temperature dependent ellipsometric studies on WO_3 thin films," *Appl. Opt.*, vol. 38, pp. 7112–7127, 1999.
[42] Z. Hussain, "Thermo optical properties and related electronic polarizabilities of MoO_3 thin films using ellipsometry," *AJEAS*, vol. 12, pp. 90–110, 2019.
[43] R. M. A. Azzam and N. M. Bashara, *Ellipsometry and Polarized Light*. Amsterdan, The Netherland: North-Holland, 1989.
[44] F. L. McCrackin, *NBS Technical Note*. U.S. Government Printing Office, Washington, D.C., 1969, vol. 479.
[45] F. L. McCrackin, E. Passaglia, R. R. Stromberg, and H. L. Steinberg, "Measurement of the thickness and refractive index of very thin films and the optical properties of surfaces by ellipsometry," *J. Res. Natl. Bureau Stand. A*, vol. 67, pp. 363–377, 1993.
[46] M. Green and Z. Hussain, "Optical properties of lithium tungsten bronze thin films," *J. Appl. Phys.*, vol. 74, pp. 3451–3458, 1993.
[47] Z. Hussain, "Optical and electrochromic properties of oxide bronze thin films," Ph.D. thesis, Univ. London, London, U.K., 2007.

[48] M. Green and Z. Hussain, "Optical properties of dilute hydrogen tungsten bronze thin films," *J. Appl. Phys.*, vol. 69, pp. 7788–7796, 1991.
[49] M. Shiojiri, T. Miyano, and C. Kaito, "Electron microscopic studies of structure and crystallization of amorphous metal oxide films," *Jpn. J. Appl. Phys.*, vol. 18, pp. 1937–1947, 1979.
[50] Y. Shigesato, "Photochromic properties of amorphous WO_3 thin films," *Jpn. J. Appl. Phys.*, vol. 30, pp. 1457–1462, 1991.
[51] K. S. Kang, "Electrochromic display: sodium insertion in tungsten trioxide films," Ph.D. Thesis, Univ. London, London, U.K., 1979.
[52] P. Gerard, A. Deneuville, G. Hollinger, and T. M. Buc, "Color in tungsten trioxide thin films," *J. Appl. Phys.*, vol. 48, pp. 4252–4255, 1977.
[53] C. Ottermann, A. Temmink, and K. Bange, "Correlation of injected charge to optical constants (n, k) of electrochromic films," *SPIE*, vol. 1272, pp. 111–121, 1990.
[54] J. Nagai and T. Kaninori, "Kinetic study of Li_xWO_3 electrochromism," *Jpn. J. Appl. Phys.*, vol. 22, pp. 681–687, 1983.
[55] P. G. Dickens, S. G. Baker, and M. T. Weller, "Hydrogen insertion in oxides," *Solid State Ionics*, vol. 18/19, pp. 89–97, 1986.
[56] P. A. Cox, M. D. Hill, F. Peplinskii, and R. G. Egdell, "2D surface phonons in high resolution electron-energy-loss spectra of metallic oxides," *Surf. Sci.*, vol. 141, pp. 13–30, 1984.
[57] E. Salje and B. Gittler, "Anderson transition and intermediate polaron formation in WO_{3-x} transport properties and optical absorption," *Philos. Mag. B*, vol. 50, pp. 607–620, 1984.
[58] Q. Zhong, J. R. Dahn, and K. Colbow, "Lithium intercalation into WO_3 and the phase diagram of Li_xWO_3," *Phys. Rev. B.*, vol. 46, pp. 2554–2560, 1992.
[59] A. W. Sleight, T. A. Bither, and P. E. Bierstedt, "Superconducting oxides of rhenium and molybdenum with tungsten bronze type structures," *Solid. State Commun.*, vol. 7, pp. 299–300, 1969.
[60] J. B. Goodenough, "Metallic oxides," *Prog. Solid State Chem.*, vol. 5, pp. 145–399, 1971.
[61] M. G. Stachiotti, F. Cora, C. R. A. Catlow, and C. O. Rodriguez, "First-principles investigation of ReO_3 sand related oxides," *Phys. Rev. B.*, vol. 55, pp. 7508–7514, 1997.
[62] H. R. Zeller and H. W. Beyler, "Electrochromism and local order in amorphous WO_3," *Appl. Phys.*, vol. 13, pp. 231–237, 1977.
[63] K. L. Ngai and R. Silberglitt, "Effect of lattice instability on superconductivity in sodium tungsten bronze," *Phys. Rev. B*, vol. 13, pp. 1032–1039, 1976.
[64] Q. Zhong, S. A. Wessel B. Heinrich, and K. Colbow, "The electrochromic properties and mechanism of H_xWO_3, Li_xWO_3," *Sol. Energy Mater.*, vol. 20, pp. 289–296, 1990.
[65] J. Gottsche, A. Hinsch, and V. Wittwer, "Electrochromic mixed WO_3 and TiO_2 thin films produced by sputtering and the sol-gel technique: A comparison," *Sol. Energy Mater. Sol. Cells*, vol. 31, pp. 415–428, 1993.
[66] F. Cora, M. G. Stachiotti, C. R. A. Catlow, and C. O. Rodriguez, "Transition metal oxide chemistry: Electronic structure study of WO_3, ReO_3, and $NaWO_3$," *J. Phys. Chem. B.*, vol. 101, pp. 3945–3952, 1997.
[67] P. J. Wiseman and P. G. J. Dickens, "The crytal structure of cubic hydrogen tungsten bronze," *J. Solid State Chem.*, vol. 6, pp. 374–377, 1973.
[68] C. J. Wright, "Inelastic neutron scattering spectra of the hydrogen tungsten bronze $H_{0.4}WO_3$," *J. Solid State Chem.*, vol. 20, pp. 89–92, 1977.
[69] M. A. Habib and S. P. Maheswari, "In situ infrared spectroscopic study of the electrochromic reactions of tungsten trioxide films," *J. Electrochem. Soc.*, vol. 138, pp. 2029–2031, 1991.
[70] M. Sato, B. H. Grier, G. Shirane, and T. Akahane, "Sucessive structural phase transitions in Na_xWO_3," *Phys. Rev. B.*, vol. 25, pp. 6876–6885, 1982.
[71] J. J. Kleperis, P. D. Cihmach, and A. R. Lusis, "Colour centres in amorhous tungsten trioxide thin films," *Phys. Status Sol. A*, vol. 83, pp. 291–297, 1984.
[72] P. A. Gillet, J. L. Fourquet, and O. Bohnke, "Niobium tungsten titanium oxides: From soft chemistry precursors to electrochromic thin layer materials," *Mater. Res. Bull.*, vol. 27, pp. 1145–1152, 1992.
[73] O. Bohnke, A. Gire, and J. G. Theobald, "In situ detection of electrical conductivity variation of an a-WO_3 thin film during electrochemical reduction and oxidation in $LiClO_4$ (M)–PC electrolyte," *Thin Solid Films*, vol. 247, pp. 51–55, 1994.
[74] M. Born and E. Wolf, *Principles of Optics*. Cambridge, U.K.: Cambridge Univ. Press, 1999.
[75] R. Jacobson, *Physics of Thin Films*. G. Hass, M. H. Francombe, and R. W. Hoffmasn, Eds., New York, NY, USA: Academic, 1971, vol. 8, pp. 51–98.
[76] M. Deepa, A. K. Srivastava, M. Kar, and S. A. Agnihotry, "A case study of optical and structure of sol-gel derived nanocrystalline electrochromic WO_3films," *J. Phys. D.*, vol. 39, pp. 1885–1893, 2006.
[77] A. H. Jayatissa, S. T. Cheng, and T. Gupta, "Annealing effect on the formation of nanocrystals in thermally evaporated tungsten oxide thin films," *Mater. Sci. Eng B.*, vol. 109, pp. 269–275, 2004.
[78] C. Y. Su, H. C. Lin, T. K. Yang, and C. K. Lin, "Structure and optical properties of tungsten oxide nanomaterials prepared by a modified plasma arc gas condensation technique," *J. Nanoparticle Res.*, vol. 12, pp. 1755–1763, 2010.
[79] B. A. H. Sanchez, T. J. Boyle, H. D. Pratt III, M. A. Rodriguez, L. N. Brewer, and D. R. Dunphy, "Morphological and phase controlled tungsten based nanoparticles: Synthesis and characterization of scheelite, wolframite, and oxide nanomaterials," *Chem. Mater.*, vol. 20, pp. 6643–6656, 2008.
[80] Y. Liu and P. H. Daum, "Relationship of refractive index to mass density and self-consistency of mixing rules for multicomponent mixtures like ambient aerosols," *Aerosol Sci.*, vol. 39, pp. 974–986, 2008.
[81] E. Hecht, *Optics*. 4th ed. New York, NY, USA: Addison Wesley, 2002.
[82] E. S. Kang, J. Y. Bae, and B. S. Bae, "Measurement of thermo-optic coefficients in sol-gel hybrid glass films," *J. Sol. Gel Sci. Technol.*, vol. 26, pp. 981–984, 2003.
[83] Y. Chai, C. W. Tam, K. P. Beh, F. K. Yam, and Z. Hassan, "Effects of thermal treatment on the anodic growth of tungsten oxide films," *Thin Solid Films*, vol. 588, pp. 44–49, 2015.

[84] C. Y. Kim and S. Park, "Electrochromic properties of WO_3 thin film with various heat-treatment temperature," *Asian J. Chem.*, vol. 25, pp. 5874–5878, 2013.
[85] C. Y. Kim, M. Lee, S. H. Huh, and E. K. Kim, "WO_3 thin film coating from H_2O- controlled per oxo tungstic acid and its electronic properties," *J. Sol. Gel. Sci. Technol.*, vol. 53, pp. 176–183, 2010.
[86] Y. Chai, C. W. Tam, K. P. Beh, F. K. Yam, and Z. Hassan, "Effects of thermal treatment on the anodic growth of tungsten oxide films," *Thin Solid Films*, vol. 588, pp. 44–49, 2015.
[87] A. H. Jayatissa, S. T. Cheng, and T. Gupta, "Annealing effect on the formation of nanocrystals in thermally evaporated tungsten oxide thin films," *Mater. Sci. Eng. B.*, vol. 109, pp. 269–275, 2004.
[88] A. Nakamura, T. Kawauchi, K. Urabe, M. Kitao, and S. Yanada, "Characterization of amorphous tungsten oxide films through optical absorption spectra," *J. Vacuum Soc. Jpn.*, vol. 24, pp. 471–475, 1981.
[89] M. A. Habib and S. P. Maheswari, "Limiting concentration of hydrogen in an electrochromic tungsten trioxide efilms," *Sol. Energy Mater. Sol. Cells.*, vol. 25, pp. 195–200, 1992.
[90] S. Darmawi *et al.*, "Correlation of electrochromic properties and oxidation states in nanocrystalline tungsten trioxide," *Phys. Chem. Chem. Phys.*, vol. 17, 2015, Art. no. 15903.
[91] I. G. Austin and N. F. Mott, "Polarons in crystalline and non-crystalline materials," *Adv. Phys.*, vol. 18, pp. 41–102, 1969.
[92] R. D. Gould and B. B. Ismail, "Observations of low temperature hopping conduction in evaporated cadmium telluride thin films using current-temperature measurements," *Phys. Status Sol (a)*, vol. 134, pp. K65–K68, 1992.
[93] T. He and J. Yao, "Photochromic materials based on tungsten oxide," *J. Mater. Chem.*, vol. 17, pp. 4547–4557, 2007.
[94] E. Iguchi, E. Salje, and R. J. D. Tilley, "Polaron interaction energies in reduced tungsten trioxide," *J. Solid State Chem.*, vol. 38, pp. 342–359, 1981.
[95] J. Ederth, A. Hoel, G. A. Niklasson, and C. G. Granqvist, "Small polaron formation in porous W_{3-x} nano particle films," *J. Appl. Phys.*, vol. 96, pp. 5722–5726, 2004.
[96] M. R. Goulding and C. B. Thomas, "The transport properties of amorphous films of tungstic oxide, sublimed under different conditions," *Thin Solid Films*, vol. 62, pp. 175–188, 1979.
[97] O. F. Schirmer and E. Salje, "Conduction bipolarons in low-temperature crystalline WO_{3-x}," *J. Phys C: Solid State Phys.*, vol. 13, pp. L1067–L1072, 1980.
[98] R. Gehlig and E. Salje, "Dielectric properties and polaronic conductivity of WO_3 and $W_xMo_{1-x}O_3$," *Philos. Mag. B.*, vol. 47, pp. 229–245, 1983.
[99] N. Bondarenko, O. Eriksson, and N. V. Skorodumova, "Polaron mobility in oxygen-deficient and lithium-doped tungsten trioxide," *Phys. Rev. B.*, vol. 92, 2015, Art. no. 165119.